ISSN 0029 - 3865

CBPF-NF-059/89

CRITICALITY OF THE DISCRETE N-VECTOR FERROMAGNET IN A CUBIC LATTICE WITH A FREE SURFACE

by

Anna CHAME and Constantino TSALLIS

Centro Brasileiro de Pesquisas Físicas - CBPF/CNPq
Rua Dr. Xavier Sigaud, 150
22290 - Rio de Janeiro, RJ - Brasil

ABSTRACT

We study a discrete N-component spin ferromagnet with Hamiltonian

$$\beta\mathcal{H} = - NK \sum_{<i,j>} (\vec{S}_i.\vec{S}_j) - N^2L \sum_{<ij>} (\vec{S}_i.\vec{S}_j)^2$$

in a semi-infinite cubic lattice. The coupling constants at the surface, K_S and L_S, are allowed to be different from the bulk ones, K_B and L_B. Using a simple real-space renormalisation group procedure we obtain the N-evolution (N real) of the phase diagram, including the $N \to 0$ and $N \to \infty$ limits. The thermal (ν) and crossover (ϕ) critical exponents at various critical and multicritical points are calculated.

Key-words: Discrete N-vector model; Surface magnetism; Renormalisation group; Critical properties.

I INTRODUCTION

Hamiltonians containing cubic anisotropic terms, which break the full rotational invariance, have been used to describe structural phase transitions in lattices with cubic symmetry[1] as well as the behaviour of some anisotropic ferromagnets[2].

The discrete N-component cubic model, which is a limit of high cubic anisotropy of such Hamiltonians, was firstly introduced[3] in relation with the tricritical-like behaviour of cubic rare earths compounds, in particular HoSb. This model can be defined in several ways. Usually it is defined by

$$-\beta\mathcal{H} = NK \sum_{<i,j>} \vec{S}_i . \vec{S}_j \quad , \tag{1}$$

with $\beta = 1/k_B T$ and where $<i,j>$ denotes pairs of nearest-neighbouring N-component spins $\vec{S}_i$. These spins can only point along the positive or negative axis directions of a N-dimensional hypercube, i.e., $\vec{S}_i = (\pm 1,0,0,\ldots),(0,\pm 1,0,\ldots), \ldots$ The model may be alternatively defined by associating with each lattice site i two discrete variables, namely, an axis variable $\alpha_i = 1,2,\ldots N$ and the Ising variable $\sigma_i = \pm 1$.

In this way Eq. (1) is equivalent to

$$-\beta\mathcal{H} = NK \sum_{<i,j>} \delta_{\alpha_i,\alpha_j} \sigma_i \sigma_j \quad . \tag{2}$$

The discrete cubic model has many realisations in two dimensions (d = 2), mainly in the field of adsorbed monolayers (for a

review see Ref. 4). For example the orientational ordering of diatomic molecules adsorbed in a triangular lattice[5] (as observed in N_2 adsorbed on graphite[6]) can be simulated by the cubic model with N = 3.

On theoretical grounds, the cubic model has been treated using several techniques, such as Mean Field theories[3], Niemeijer-van Leeuwen renormalisation group (RG)[7], Migdal RG[8], variational RG[9], Monte Carlo-like approach[10], conformal invariance[11] and Monte Carlo RG[12].

Using a real space RG procedure which preserves the correlation function, an extended N-component cubic model with dimensionless Hamiltonian

$$-\beta\mathcal{H} = NK \sum_{<i,j>} \vec{S}_i.\vec{S}_j + N^2L \sum_{<i,j>} (\vec{S}_i.\vec{S}_j)^2 \qquad (3)$$

was recently studied in a square lattice[13]. Using the notation of Eq. (2), the Hamiltonian of Eq. (3) is equivalent to

$$-\beta\mathcal{H} = NK \sum_{<i,j>} \sigma_i\sigma_j\delta_{\alpha_i,\alpha_j} + N^2L \sum_{<i,j>} \delta_{\alpha_i,\alpha_j} \quad . \qquad (4)$$

Besides the fact that this extended model presents several interesting limiting cases, another motivation to study it is, as we shall see later on, that the Hamiltonian of Eq. 3 remains closed for all N under this kind of RG, whereas that of Eq. 1 does not.

In the present work, we consider the model given by Eq. (3) in a cubic lattice with a free surface. The coupling constants

at the free surface, K_s and L_s are allowed to be different from the bulk ones K_B and L_B. Using simple diamond cells, we obtain the phase diagrams, for arbitrary values of N, in the (K_B, L_B, K_S, L_S) parameter space as well as the various thermal (ν) and crossover (ϕ) critical exponents.

This paper is divided as follows: in section II we present the model and the RG formalism, in section III our results and, finally, we conclude in section IV.

II MODEL AND RG FORMALISM

We will consider the generalised version of the discrete cubic model, given by Eq. (3). Let us review some important particular cases and features of this model. We note that the Hamiltonian as given by Eq. (4), for $K = 0$, corresponds to the N-state Potts model with dimensionless coupling constant N^2L. Also in the $N \to 0$ limit, the self-avoiding walk problem is obtained[7] with step fugacity K. For $N = 1$, Eq. (4) reduces to the spin 1/2 Ising model for all values of L. For $N = 2$, the Z(4) model is recovered (see Ref. 14 and references therein). In the case $K = NL$, we can see that we obtain the 2N-state Potts model with coupling constant 2NK. For finite K and $NL/|K| \to \infty$, the second term in Eq. (4) becomes dominant, and one of the N axes is preferentially chosen, consequently the spin 1/2 Ising model with coupling constant NK is recovered.

Let us now focus on some results. It was conjectured that the Mean Field approach is exact in the $N \to \infty$ limit[10] if $L = 0$. Similarly to what happens for the Potts ferromagnet, a first order transition is expected (on a Bravais lattice) for $N > N_c$. Mean Field theory predicts[3] that the model given by Eq. 2, for $d = 3$, exhibits a first order transition for $N > 3$; series results[15] indicate that already for $N = 3$ the transition is first order. For the model given by Eq. 4, for $d = 3$, several types of transitions occur (as will be seen later on), which correspond to different universality classes: the 2N-state Potts transition, which is a first order one for $2N \gtrsim 3$, the N-state Potts transition, which is a first order one for $N \gtrsim 3$ and the Cubic transition, whose first or second order nature is believed[9] to depend on the ratio L/K if $1.1 < N < 3.4$, and is a first order one for values of N above 3.4. We will not be concerned here with first order phase transitions, which have already been studied, for $d = 2$, employing the vacancy technique within a RG framework[9]. The present RG will be exact for hierarchical lattices, which do not present first order transitions for the cubic model. Therefore, the present results will be relevant for Bravais lattices only for $N \lesssim N_c$ (N_c depends on the particular transition).

Let us now briefly review the phase diagram of the $d = 2$ system (which is qualitatively equal to the $d = 3$ case, as will be shown later on). It presents three distinct phases. For low values of both K and L, we have the *paramagnetic* (P) phase, where the spins $\vec{S}_i$ are disordered. For relatively high values of both K and L, the *ferromagnetic* (F) phase appears (in this case the spins $\vec{S}_i$ are preferentially ordered along one of the 2N directions). For low values of K and intermediate values of L, a new

phase appears, namely, the *intermediate* (I) phase, where the spins $\vec{S}_i$ are preferentially aligned along one of the N axes of the hypercube but there is no preference concerning the orientation along this axis. In Fig. 1a we show the phase diagram as obtained in[16] for the cubic model in a square lattice (N = 3). In Fig. 1b we also display a typical phase diagram (Wheatstone-bridge hierarchical lattice, N = 2), as obtained in[13], where a convenient variable has been used, namely the *vector thermal transmissivity* (t_1,t_2) (see Ref. 13 and references therein) with

$$t_1 \equiv \frac{1 - e^{-2NK}}{1 + 2(N-1)e^{-N(K+NL)} + e^{-2NK}} \quad , \tag{5.a}$$

$$t_2 \equiv \frac{1 - 2e^{-N(K+NL)} + e^{-2NK}}{1 + 2(N-1)e^{-N(K+NL)} + e^{-2NK}} \quad , \tag{5.b}$$

It will be useful to present also the inverse relations, namely

$$e^{-N(K+NL)} = \frac{1 - t_2}{1 + Nt_1 + (N-1)t_2} \quad , \tag{6.a}$$

$$e^{-2NK} = \frac{1 - Nt_1 + (N-1)t_2}{1 + Nt_1 + (N-1)t_2} \quad , \tag{6.b}$$

Within the RG frameworks[13,16], the atractors (trivial fixed points) of the paramagnetic, ferromagnetic and intermediate phases are respectively located at $(t_1,t_2) = (0,0),(1,1)$ and $(0,1)$ which correspond to $(K,L) = (0,0),(\infty,\infty)$ and $(0,\infty)$. The semi-stable fixed point $\mathcal{S}$ (see Fig. 1), associated with the transition from the intermediate to the ferromagnetic phase (in which the spins $\vec{S}$ preferentially align in one sense along a previously chosen

axis), has the Ising character. Similarly, the other two semi-stable fixed points in this diagram, namely $\mathcal{P}(N)$ (N-state Potts fixed point) and $\mathcal{C}$ (cubic fixed point) are respectively associated with the transitions from the paramagnetic to the intermediate phase (one out of N axes is chosen) and from the paramagnetic to the ferromagnetic phase (one axis and one sense in this axis are chosen). The fully unstable fixed point $P(2N)$ $(t_1 = t_2)$ corresponds to $K = NL$, then, as we noted before, we have the 2N-state Potts critical behaviour. For $N > N^*$, an interchange of stability occurs for the $\mathcal{C}$ and the $P(2N)$ fixed points[13,16].

The presence of a surface in this problem introduces new possibilities of order. In general, this order will depend on the ratios of the surface and bulk coupling constants. For instance, the phase diagram for the Ising ferromagnet in a cubic lattice with a free surface (0,0,1) is known to be as indicated in Fig. 2(a). If $\Delta \equiv K_S/K_B - 1 < \Delta_c$, for temperatures below the critical bulk temperature T_c^B (corresponding to $1/K_B^c$ in Fig. 2(a)) we have the *bulk ferromagnetic* (BF) phase, where both the bulk and the surface are ordered; for $T > T_c^B$ we have the *paramagnetic* (P) phase, where both are disordered. If $\Delta > \Delta_c$, another phase appears for intermediate values of T($T_c^B < T < T_c^S(\Delta)$), in which the surface remains ordered while the bulk is completely disordered (*surface ferromagnetic* (SF) phase). In Fig. 2(b) we show the phase diagram as obtained in[17], where the transmissivities $t_B \equiv \text{tgh } K_B$ and $t_s = \text{tgh } K_s$ have been used. If we look at the correlation length in a semi-infinite ferromagnet, we expect the following critical exponents: whereas the bulk correlation length diverges as $|T - T_c^B|^{-\nu^{3D}}$ for all values of Δ, the surface

correlation length diverges, on the P - BF line ($\Delta < \Delta_c$), as $|T - T_c^B|^{-\nu_1}$, and, on the P-SF line ($\Delta > \Delta_c$) as $|T - T_c^S(\Delta)|^{-\nu^{2D}}$. In addition, a soft singularity might be present in the surface correlation length on the BF - SF line ($\Delta > \Delta_c$). In the vicinity of the multicritical point ($\Delta \to \Delta_c + 0$), we expect $(T_c^S(\Delta)/T_c^B - 1) \alpha (\Delta/\Delta_c - 1)^{1/\phi}$, which defines the crossover exponent ϕ. Here we will be concerned with thermal exponents associated with bulk transitions (similar to ν^{3D}) and with surface transitions (similar to ν^{2D}), as well as the crossover exponents ϕ at the various multicritical points.

In the present work we consider a discrete cubic ferromagnet (given by Eq. (3)) in a semi-infinite cubic lattice with a (0,0,1) free surface. The nearest-neighbour interactions are characterised by the dimensionless coupling constants K_s and L_s ($K_S > 0$ and $K_S + NL_S > 0$) if both sites i and j belong to the surface, and by K_B and L_B ($K_B > 0$ and $K_B + NL_B > 0$) otherwise.

To obtain the phase diagrams in the four-dimensional space (K_B, L_B, K_S, L_S), we consider the RG transformations of Fig. 3, similarly to the Migdal-Kadanoff approach used by Domany and Riedel[8]. The diamond cells which we have adopted proved satisfactory for surface magnetism in the Potts model[17]. The large two-rooted graph shown in Fig.3(a) approaches, through the standard bond-moving procedure, the bulk of the cubic lattice. The large graph of Fig. 3(b) approaches, in the same way, the surface region of our system, where the dashed bonds represent the free surface interactions. The graph of Fig. 3(b) may be viewed as that of Fig. 3(a) laying with its two terminals on the free surface, nine missing bonds in the vacuum, nine on the surface and nine in the bulk. The recurrence relations for (K_B, K_s, L_B, L_s) are obtained by imposing that, under renormalisation, the correlation function between the two terminals is preserved (see Ref. 18). It has been shown[13] that this procedure is connected with the phenomenological RG approach. We have, for the bulk transformation (Fig. 3(a)), that

$$e^{-\beta \mathcal{H}'_{B_{12}}} = \underset{1,2,3,\ldots 20}{Tr}\, e^{-\beta \mathcal{H}_{B_{123\ldots 20}}} , \qquad (7.a)$$

and for the surface one (Fig. 3(b)), that

$$e^{-\beta \mathcal{H}'_{S_{12}}} = \underset{1,2,3,\ldots,14}{Tr}\, e^{-\beta \mathcal{H}_{S_{123\ldots 14}}} , \qquad (7.b)$$

with

$$-\beta \mathcal{H}'_{B_{12}} = NK'_B \vec{S}_1.\vec{S}_2 + N^2 L'_B (\vec{S}_1.\vec{S}_2)^2 + K^0_B \qquad (8.a)$$

(associated with graph G'_1),

$$-\beta \mathcal{H}_{B_{123..20}} = NK_B (\vec{S}_1.\vec{S}_5 + \vec{S}_1.\vec{S}_7 + \ldots + \vec{S}_{20}.\vec{S}_2)$$

$$+ N^2 L_B ((\vec{S}_1.\vec{S}_5)^2 + (\vec{S}_1.\vec{S}_7)^2 + \ldots + (\vec{S}_{20}.\vec{S}_2)^2) \qquad (8.b)$$

(associated with graph G_1) ,

$$-\beta \mathcal{H}'_{S_{12}} = NK'_S (\vec{S}_1.\vec{S}_2) + N^2 L'_S (\vec{S}_1.\vec{S}_2)^2 + K^0_S \qquad (8.c)$$

(associated with graph G'_2) and

$$-\beta \mathcal{H}_{S_{123..14}} = NK_S (\vec{S}_1\vec{S}_3 + \vec{S}_1.\vec{S}_5 + \ldots + \vec{S}_{14}.\vec{S}_2)$$

$$+ N^2 L_S ((\vec{S}_1\vec{S}_3)^2 + (\vec{S}_1.\vec{S}_5)^2 + \ldots + (\vec{S}_{14}.\vec{S}_2)^2)$$

$$+ NK_B(\vec{S}_1.\vec{S}_9 + \vec{S}_1.\vec{S}_{11} + \ldots \vec{S}_{14}.\vec{S}_2) + N^2L_B((\vec{S}_1.\vec{S}_9)^2$$

$$+ (\vec{S}_1.\vec{S}_{11})^2 + \ldots(\vec{S}_{14}.\vec{S}_2)^2) \quad . \tag{8.d}$$

(associated with graph G_2), where K_B^o and K_S^o are additive constants to be determined.

Equations (7) uniquely determine K_B', L_B', K_S', L_S'. These recurrence relations may be equivalently obtained using the vector thermal transmissivities defined in Eq. (5). In fact, we have established the effective bulk and surface vector transmissivities for this problem, using its series and paralel composition rules and the definition of its dual[13].

For the bulk transformation we have obtained

$$\frac{1 - t'_{2B}}{1 + Nt'_{1B} + (N-1)t'_{2B}} = \left(\frac{1 - t^3_{2B}}{1 + Nt^3_{1B} + (N-1)t^3_{2B}}\right)^9 \tag{9.a}$$

and

$$\frac{1 - Nt'_{1B} + (N-1)t'_{2B}}{1 + Nt'_{1B} + (N-1)t'_{2B}} = \left(\frac{1 - Nt^3_{1B} + (N-1)t^3_{2B}}{1 + Nt^3_{1B} + (N-1)t^3_{2B}}\right)^9 \quad ; \tag{9.b}$$

For the surface transformation, we have obtained

$$\frac{1 - t'_{2S}}{1 + Nt'_{1S} + (N-1)t'_{2S}} = \left(\frac{1 - t^3_{2S}}{1 + Nt^3_{1S} + (N-1)t^3_{2S}}\right)^3 \left(\frac{1 - t^3_{2B}}{1 + Nt^3_{1B} + (N-1)t^3_{2B}}\right)^3$$

(9.c)

and

$$\frac{1-Nt'_{1S}+(N-1)t'_{2S}}{1+Nt'_{1S}+(N-1)t'_{2S}}=\left(\frac{1-Nt^3_{1S}+(N-1)t^3_{2S}}{1+Nt^3_{1S}+(N-1)t^3_{2S}}\right)^3\left(\frac{1-Nt^3_{1B}+(N-1)t^3_{2B}}{1+Nt^3_{1B}+(N-1)t^3_{2B}}\right)^3 \tag{9.d}$$

Iterating $(t'_{1B},t'_{2B},t'_{1S},t'_{2S})$ as functions of $(t_{1B},t_{2B},t_{1S},t_{2S})$ given by Eqs. (9), we obtain for fixed N the RG flow which will determine the fixed points, the phase diagram, as well as the universality classes with their corresponding critical exponents. To obtain the exponents ν and ϕ we calculate the Jacobian matrix $\partial(t'_{1B},t'_{2B},t'_{1S},t'_{2S})/\partial(t_{1B},t_{2B},t_{1S},t_{2S})$ on the various semi-stable or fully unstable fixed points. In general, we perform this calculation on invariant planes, whose corresponding Jacobian is a 2 x2 matrix. Denoting its eigenvalues by λ_1 and λ_2, we have (i) for the semi-stable fixed points, $\lambda_1>1>\lambda_2$ and

$$\nu=\frac{\ell nB}{\ell n\lambda_1} \quad , \tag{10}$$

where B is the linear expansion factor (for our transformation, B = 3);

(ii) for the fully unstable fixed points, $\lambda_1 > 1$ and $\lambda_2 > 1$, and

$$\nu_S=\frac{\ell nB}{\ell n\lambda_S} \qquad (S \neq 1,2) \quad , \tag{11}$$

$$\phi=\frac{\ell n\lambda_2}{\ell n\lambda_1} \quad , \tag{12}$$

where $\lambda_1 > \lambda_2$. As mentioned before, the thermal critical exponent will correspond to the bulk or surface correlation length, according to the nature of the respective fixed point.

III RESULTS

We find, for arbitrary finite N, the following fully stable fixed points $(t_{1B}, t_{2B}, t_{1S}, t_{2S})$:

(i) (0,0,0,0), which corresponds to $K_B = L_B = K_S = L_S = 0$, characterizing the *paramagnetic* (P) *phase*;

(ii) (1,1,1,1), corresponding to $K_B = L_B = K_S = L_S \to \infty$, characterizing the *bulk ferromagnetic* (BF) *phase*. Both bulk and surface have their spins preferentially aligned along one axis and one orientation in this axis;

(iii) (0,1,0,1), corresponding to $K_B = 0$, $L_B \to \infty$, $K_S = 0$, $L_S \to \infty$, characterizing the *bulk intermediate* (BI) *phase*. Both bulk and surface have their spins preferentially aligned along one axis, without restriction about the orientation along this axis;

(iv) (0,1,1,1), corresponding to $K_B = 0$, $L_B \to \infty$, $K_S \to \infty$, $L_S \to \infty$, characterizing the *surface ferromagnetic/bulk intermediate phase* (SFBI). In this phase, the surface remains ferromagnetically ordered while the bulk mantains only an intermediate order;

(v) (0,0,1,1), corresponding to $K_B = 0$, $L_B = 0$, $K_S \to \infty$, $L_S \to \infty$, characterizing the *surface ferromagnetic phase* (SF). We have a paramagnetic bulk while the surface is ferromagnetically ordered;

(vi) (0,0,0,1), corresponding to $K_B = 0$, $L_B = 0$, $K_S = 0$, $L_S \to \infty$, characterizing the *surface intermediate* (SI) *phase*. We have an intermediate ordered surface and a paramagnetic bulk.

We note that it is not possible for the surface to be in a less ordered phase than the corresponding bulk phase: the bulk order induces surface order (while the opposite is not true).

For all arbitrary finite values of N we find that $t_{1B} = 0$, $t_{2S} = 1$ and $t_{2B} = 1$ are subspaces which remain invariant under renormalisation. These invariant cubes are shown (for N = 2) in Figs. 4,5 and 6, respectively. As we have used the transmissivities, a non-physical region (complex coupling constants) appears in those figures. The non-physical region is given by

$$1 \pm Nt_{1B} + (N-1)t_{2B} < 0 \quad ,$$

$$1 \pm Nt_{1S} + (N-1)t_{2S} < 0 \quad , \qquad (13)$$

$$1 - t_{2B} < 0$$

and $$1 - t_{2S} < 0 \quad .$$

For $t_{1B} = 0$ ($K_B = 0$) we only have the second term in the bulk Hamiltonian, i.e., we have the N-state Potts model for the bulk and the N-cubic model for the surface. This is a quite interesting case, as it may be applied to describe a semi-infinite Potts system with an adsorbed monolayer on its free surface.

Five different phases appears in the unitary cube of Fig. 4, namely the P, BI, SFBI, SF and SI ones. We also notice that the critical behaviours associated with *all* the internal critical points in this cube are governed by the fixed (critical) points in the "walls" $t_{2B} = 0$, $t_{1S} = 0$ and $t_{2S} = 1$ (see Table 1).

For $t_{2S} = 1$ ($L_S \to \infty$) (see Fig. 5) the second term in the surface Hamiltonian is dominant, hence all the surface spins are aligned along one axis. We recover the spin 1/2 Ising model at the surface while the bulk remains associated with the cubic model. Five phases are presented in this unitary cube, namely the SF,SFBI,SI,BI and BF ones (see also Table 1). We note that in this cube there is an invariant line corresponding to $t_{1B} = t_{2B} \cong 0.31$ where we have for all values of t_{1S} three coexisting phases (either SF/SFBI/BF or SI/BI/BF). Along this line we have a fully unstable fixed point $(t_{1B},t_{2B},t_{1S},t_{2S}) = (0.31,0.31,0.48,0.48)$ where the five present phases coexist. We will turn back to this point later on.

For $t_{2B} = 1$ ($L_B \to \infty$) (see Fig. 6) the second term in the bulk Hamiltonian is dominant, hence all the bulk spins are aligned along one axis. Now the surface remains associated with the cubic model while we recover the spin 1/2 Ising model for the bulk. The phases corresponding to a completely disordered bulk do not appear and we only have three phases, namely the BI, BF and SFBI ones. For this unitary cube, the plane $t_{2B} = 1$, $t_{2S} = 0$ goes, at the first RG iteration, into the plane $t_{2S} = t_{2B} = 1$.

Estimates for the critical thermal exponents ν^{3D} and ν^{2d} at the fixed (critical) points which govern the various transitions in those

cubes are presented in Table 1 for typical values of N. From these values we notice that the SI-SF and the SFBI-BI transitions belong, for all N, to the same universality class, namely the surface Ising one. Analogously the BF-BI and the BF-SFBI transitions belong to the bulk Ising universality class. For a given N, the SF-SFBI, BI-SI and BI-P transitions belong to the bulk N-Potts universality class. Analogously the BF-SF and the P-BF transitions belong to the bulk Cubic universality class.

For all finite values of N we have a class of invariant planes which arises from the bulk fixed points (see Table 2). This is due to the fact that the recurrence relations for t'_{1B} and t'_{2B} involve only t_{1B} and t_{2B}. We show these invariant planes in Fig. 7, for N = 2. The bulk fully stable fixed points $(t_{1B}, t_{2B}) = (0,0), (0,1)$ and $(1,1)$ give rise respectively to the phase diagrams (a), (b) and (c). We identify these planes as "walls" of the $t_{1B} = 0$ ((a) and (b)) and the $t_{2B=1}$ ((c)) cubes. The bulk (critical) fixed points $\mathcal{P}(2N)$, $\mathcal{L}$, $\mathcal{P}(N)$ and $\mathcal{J}$ give rise respectively to the planes (d), (e), (f) and (g). These planes are part of the *critical* hyper-surface in our four-dimensional space (the associated transitions are indicated in the figure). We note, in plane (c), that the P-BF transition and the fixed (critical) point which characterizes it has not appeared before (see Table 1). For $N \geq 3$ the structure of this plane is different from that for $N < 3$ (Fig. 7(e)), as shown in Fig. 7(h) ($N = 3$). We observe that, for $N \geq 3$, the BF-SI critical surface disappears. Plane (d) corresponds to critical surfaces where we have *three* coexisting phases (indicated in the figure). This

can be alternatively observed in the cube $t_{2S=1}$, where we have the line $t_{1B} = t_{2B} = 0.30792$ along which three phases coexist (SF/SFBI/BF or SI/BI/BF). The vicinity of this line, inside the critical surface, is attracted under renormalisation by fixed points at the lines $(t_{1B},t_{2B}) = (0.34,0.12)$, $(t_{1B},t_{2B}) = (0,0.34)$ or $(t_{1B},t_{2B}) = (0.34,1)$. This indicates that, *inside* the critical hyper-surface, the plane (d) is unstable with respect to the variables t_{1B} and t_{2B}, whereas the planes (e), (f) and (g) are stable.

For all finite values of N, we also have the invariant plane $t_{1S} = t_{2S} = 1$ ($K_S = L_S \to \infty$, completely ordered suface). This plane is shown in Fig. 7 (i), for N = 2.

Let us now focus on a different set of invariant planes which involve both bulk and surface variables. They are (see Fig. 8, for N = 2): (a) $t_{1B} = t_{1S} = 0$ ($K_B = K_S = 0$, which corresponds to the N-state Potts model); (b) $t_{2B} = t_{2S} = 1$ ($L_B, L_S \to \infty$, which corresponds to the Ising problem); (c) $t_{1B} = 0$, $t_{2S} = 1$ ($K_B = 0$, $L_S \to \infty$, which corresponds to an Ising surface and a N-Potts bulk) and (d) $t_{1B} = t_{2B}$, $t_{1S} = t_{2S}$ ($K_B = NL_B$, $K_S = NL_S$, which corresponds to the 2N-state Potts model). The cases (a), (b) and (d) present a familiar structure (see Fig. 2): three phases join at a multicritical point, one of them being a surface phase. The semi-stable fixed points of case (d) are associated with the coexistence of three phases, as indicated in the figure. The case (c) presents a different structure, since four phases are present. Various semi-stable fixed points are indicated in Table 1.

In Fig. 9 we present the N-evolution of the phase diagram in standard variables (a) $1/L_B$ and L_S/L_B ($\Delta_a \equiv \frac{L_S}{L_B} - 1$); (b) $1/K_B$ and K_S/K_B ($\Delta_b \equiv \frac{K_S}{K_B} - 1$); (c) $1/L_B$ and K_S/L_B ($\Delta_c \equiv \frac{K_S}{L_B} - 1$) and (d) $1/K_B$ and K_S/K_B ($\Delta_d \equiv K_S/K_B - 1$). The cases of Figs. 9(a),(b) and (d) are quite similar: for $\Delta_i < \Delta_{ic}$ we have two possible phases depending on the value of the temperature T (below or above the bulk critical temperature); for $\Delta_i > \Delta_{ic}$, a surface phase appears for intermediate temperatures. Notice in Fig. 9(b) that the phase diagrams associated with all values of N can be represented by only one diagram by using $1/NK_B$ (instead of $1/K_B$). This is due to the fact that one out of N axes has been chosen (L_B, $L_S \to \infty$), and consequently the problem is driven, for all N, to the Ising model (N = 1). In diagram (c), as we raise the temperature, the system can evolve in two ways: if $\Delta < \Delta_c$ the system changes from the SFBI into the BI and then into the SI phase; if $\Delta > \Delta_c$, it changes from the SFBI into the SF and then into the SI phase. It is worthy to stress that in the cases (b) and (c) the conditions are such that the ultimate transition of the entire system towards the paramagnetic phase occurs at infinite temperature.

In Tables 3,4,5 and 6 we present, for typical values of N and for the diagrams of Fig. 9, our estimates for the Δ_c's, critical bulk couplings, critical thermal exponents and, for the multicritical points, the crossover exponent ϕ. We note that for a given N, the value of ν^{3D} at the multicritical points on diagrams (a) and (c) is the same, corresponding to the bulk N-Potts universality class.

To discuss the $N \to \infty$ limit let us first consider the infinite

bulk case. We verify that the paramagnetic phase collapses on the $t_{1B} = t_{2B} = 0$ corner (see Fig. 1(b)). Also the IF critical line becomes a curve which simply joins the $t_{1B} = t_{2B} = 0$ corner to the $\mathcal{J}$ point (see Table 2). If we now turn back to the semi-infinite bulk case, we can see that the above mentioned collapse implies the non-existence, in this limit, of the planes generated by the $\mathcal{P}(N)$, $\mathcal{P}(2N)$ and $\mathcal{C}$ fixed points. The plane generated by the bulk fixed point $(t_{1B},t_{2B}) = (0,0)$ (Fig. 7(a)) presents only the SI and SF phases, the P phase collapses on $(t_{1B},t_{2B},t_{1S},t_{2S}) = (0,0,0,0)$ (see Fig. 7(a)). There is only one non-trivial fixed point, the one on the line $t_{2S}=1$. The same structure is mantained in the diagrams of Figs.7(b),(c) and (g). In the limit $N\to\infty$, the P and SI phases, in the diagram of Fig. 8(a), collapse respectively on the point $t_{2B}=t_{2S}=0$ and on the line $t_{2B}=0$. The same structure is maintained in the diagram of Fig. 8(b). In the diagram of Fig. 8(c) the SF and SI phases collapse respectively on the lines $t_{2B}=0$, $t_{1S}>0.62$ and $t_{2B}=0$, $t_{1S}<0.62$. In the diagram of Fig.8(d), the P and SF phases collapse, respectively, on the point $t_{1B}=t_{1S}=0$ and on the line $t_{1B}=0$.

The $N \to 0$ limit is a special case, as it recovers the self-avoiding walk (SAW) problem[7], if the coupling constants L_B and L_S are zero. In fact, the L-terms in the Hamiltonian given by Eq. (3) are proportional to N^2 and will anyhow become neglectable with respect to the K-terms (proportional to N) in the $N \to \infty$ limit. The recurrence relations become

$$K_B' = 9K_B^3 \quad ,$$

$$K_S' = 3(K_B^3 + K_S^3) \quad . \tag{14}$$

For an infinite bulk we find $K_B^c = 1/3$ and the associated critical exponent $\nu^{3D} = 1$. For the semi-infinite bulk we obtain the phase diagram shown in Fig. 10, with the disordered, surface ordered and bulk ordered phase. At the multicritical point (special transition), $\Delta_c = K_S^c/K_B^c - 1 = 0.53$ and $1/K_B^c = 3$. The thermal critical exponent associated is $\nu^{3D} = 1$ and $\phi^{-1} = 1.29$. At the fixed point $(K_B, K_S) = (1/3, 0.12)$ (ordinary transition), we have $\nu^{3D} = 1$ and at the fixed point $(K_B, K_S) = (0, 0.58)$ (surface transition), $\nu^{2D} = 1$.

IV CONCLUSIONS

We have studied surface effects in a discrete N-vector ferromagnet in a semi-infinite cubic lattice. The phase diagram presents six phases, namely the paramagnetic (P), the bulk ferromagnetic (BF), the bulk intermediate (BI), the surface ferromagnetic/bulk intermediate (SFBI), the surface ferromagnetic (SF) and the surface intermediate (SI) ones. In all cases we verify that the surface is not less ordered than the bulk. We found various invariant subspaces which we analised in detail. We have obtained the N-evolution of the critical thermal exponent for the various transitions which occur. These estimates indicate that the SI-SF and the SFBI-BI transitions belong, for all N, to the same universality class as well as the BF-BI and the BF-SFBI transitions. Furthermore, for a given N, the SF-SFBI, BI-SI and BI-P transitions belong to the same universality class,

the same occurs with the BF-SF and the P-BF transitions.

In the particular case $L_B, L_S \to \infty$, we recover the results found in Ref. 17 for the semi-infinite Ising ferromagnet. The N-state Potts semi-infinite ferromagnet is recovered in the case $K_B = K_S = 0$. In Tables 1,3 and 4 we compare our estimates for ν, ϕ and Δ_c with the ones found in Ref. 19 where more sophisticated RG clusters have been used used for this model. As we can see through the series and Monte Carlo results (which also are in Tables 1,3 and 4) we can consider our estimates for the exponents as qualitatively correct for Bravais lattices (in particular in what concerns the N-evolution of the various relevant quantities).

The general features of the phase diagrams obtained here agree with known results (whenever available) for Bravais lattices and are consistent with what might be expected for this problem, which in fact is herein studied for the first time. Let us mention an unexplained feature which occurs for the invariant plane generated by the bulk cubic fixed point: its structure is different depending on whether N is less (Fig. 7(e)) or greater (Fig. 7(h)) than N = 3, in our approach.

Our results concern only second order phase transitions. Our calculations then approximate, for $N \leq N_c$ (N_c depends on the particular transition), the results for a Bravais lattice. Nevertheless, for the hierarchical lattice associated with the RG transformation, all the present results are exact for all N.[t]

We gratefully acknowledge E.V. L. de Mello, S. Coutinho, E.P. S. da Silva and M.L. Martins for useful remarks. One of us (A.C.) has been supported by a CNPq Fellowship.

CAPTION FOR FIGURES AND TABLES

Figure 1 - (a) Phase diagram[16] for the Cubic ferromagnet, N= 3, in a square lattice: P,F and I respectively denote the paramagnetic, ferromagnetic and intermediate phases. (b) Diagram for the Wheatstone-bridge hierarchical lattice, N = 2, in the (t_1, t_2) space. The arrows indicate the RG flow; ■, ● and O respectively denote fully stable, semi-stable and fully unstable fixed points.

Figure 2 - (a) Phase diagram for the Ising ferromagnet in the semi-infinite cubic lattice with a (0,0,1) surface: P, BF and SF respectively denote the paramagnetic, bulk ferromagnetic and surface ferromagnetic phases. (b) Phase diagram in the (t_B, t_S) space. The RG flow is indicated. ■, ●, and O respectively denote fully stable, semi-stable and fully unstable fixed points.

Figure 3 - RG cell transformation: (a) for the bulk (each bond is associated with coupling constants K_B and L_B); (b) for the free surface (each dashed bond is associated with coupling constants K_S and L_S).

Figure 4 - Cube $t_{1B} = 0$ (N = 2). The entire region inside the dashed lines is non-physical. The RG flows are indicated; ■, ● and O respectively denote fully stable, semi-stable and fully unstable fixed points.

Figure 5 - Cube $t_{2S} = 1$ (N = 2).

Figure 6 - Cube $t_{2B} = 1$ (N = 2).

Figure 7 - Invariant planes generated by the infinite bulk fixed

points. Phase diagrams (N = 2) corresponding to (a) $(t_{1B}, t_{2B}) = (0,0)$; (b) $(t_{1B}, t_{2B}) = (0,1)$; (c) $(t_{1B}, t_{2B}) = (1,1)$. Critical regions (N = 2) corresponding to (d) $(t_{1B}, t_{2B}) = P(2N)$; (e) $(t_{1B}, t_{2B}) = \mathcal{E}$; (f) $(t_{1B}, t_{2B}) = P(N)$; (g) $(t_{1B}, t_{2B}) = \mathcal{F}$ (the associated transitions are indicated). (h) Critical region, for N = 3, corresponding to $(t_{1B}, t_{2B}) = \mathcal{E}$. (i) Phase diagram (N = 2) corresponding to $(t_{1S}, t_{2S}) = (1,1)$. The non-physical region is at the right of the dashed lines.

Figure 8 - Phase diagrams (N = 2) for (a) $t_{1B} = t_{1S} = 0$; (b) $t_{2B} = t_{2S} = 1$; (c) $t_{1B} = 0$, $t_{2S} = 1$ and (d) $t_{1B} = t_{2B}$, $t_{1S} = t_{2S}$.

Figure 9 - For typical values of N, the same diagrams of Fig. 8, in standard variables.

Figure 10 - $N \to 0$ limit: (a) K_S versus K_B phase diagram (the RG flow is indicated); (b) $1/K_B$ versus K_S/K_B phase diagram.

Table 1 - N-evolution of the fixed points $(t^*_{1B}, t^*_{2B}, t^*_{1S}, t^*_{2S})$ which characterise the various transitions, with the corresponding exponents ν. * denotes the results obtained in Ref. 19, [a] Ref. 20, [b] Ref. 21, [c] Ref. 22. The symbol § denotes a collapse between an unstable and a stable fixed point.

Table 2 - Infinite bulk fixed points, for typical values of N, obtained through the bulk RG transformation of Fig. 3(a). The interchange of stability for the $\mathcal{E}$ and $\mathcal{P}(2N)$ fixed points occurs for $N = N^* \cong 13$ in our approach.

Table 3 - RG estimates for the quantities associated with the multicritical point on the diagram of Fig. 9(a) ($t_{1B} = t_{1S} = 0$ or

$K_B = K_S = 0$), for typical values of N. *denotes the results obtained in Ref. 19; [d] Ref.23, [e] Ref. 24, [f] Ref. 25. For § see caption of Table 1.

Table 4 - RG estimates for the quantities associated with the multicritical point on the diagram of Fig. 9 (b) ($t_{2B} = t_{2S} = 1$ or $L_B, L_S \to \infty$); these estimates are N-independent.

Table 5 - RG estimates for the quantities associated with the multicritical point on the diagram of Fig. 9(c) ($t_{1B} = 0, t_{2S} = 1$ or $K_B = 0$, $L_S \to \infty$), for typical values of N. For § see caption of Table 1.

Table 6 - RG estimates for the quantities associated with the multicritical point on the diagram of Fig. 9(b) ($t_{1B} = t_{2B}$, $t_{1S} = t_{2S}$ or $K_B = NL_B, K_S = NL_S$). Estimates for the semi-stable fixed points and corresponding thermal exponents, respectively associated with the coexistence of the phases P-SI-SF, SF-SFBI-BF and P-BI-BF. For § see caption of Table 1.

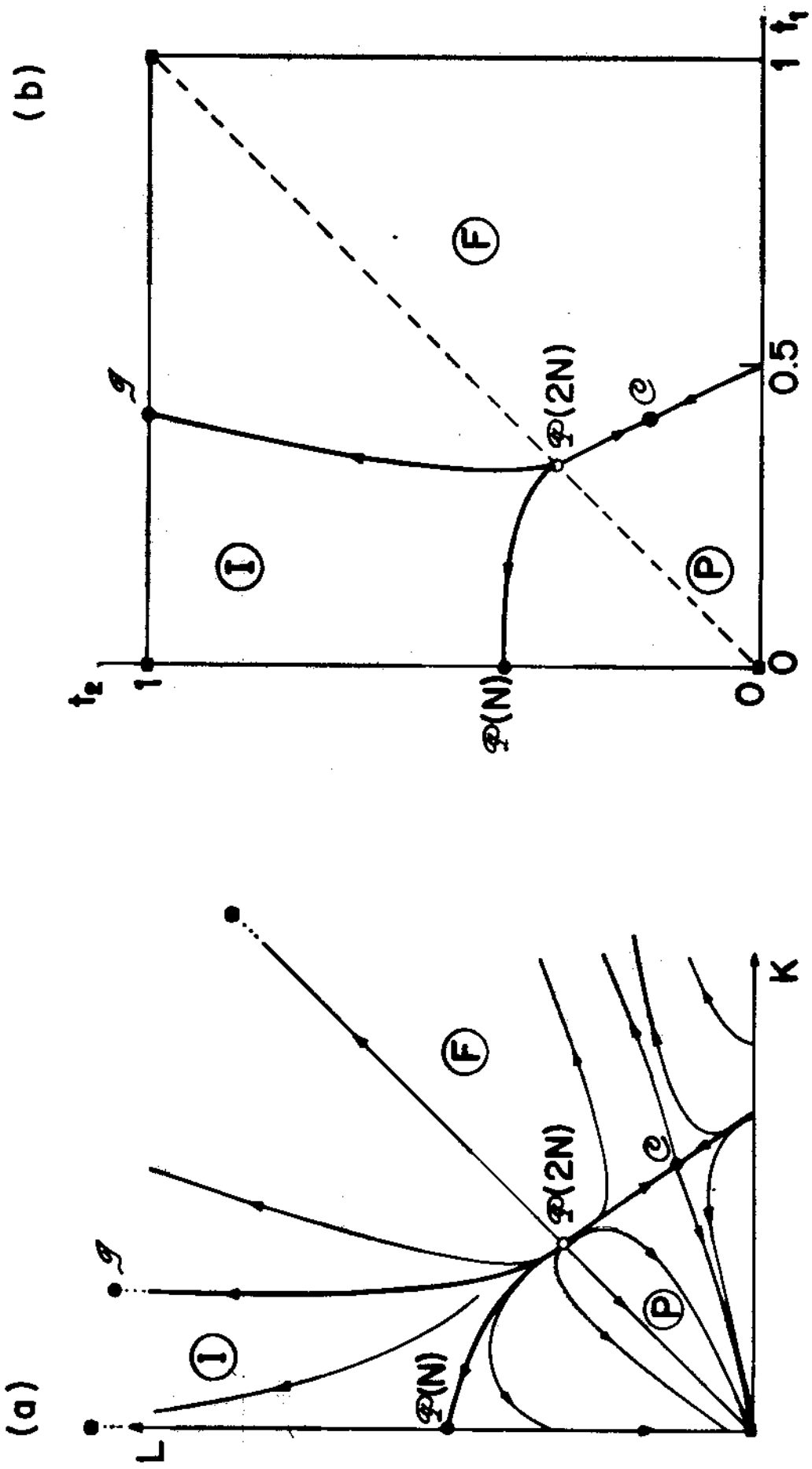

FIG.1

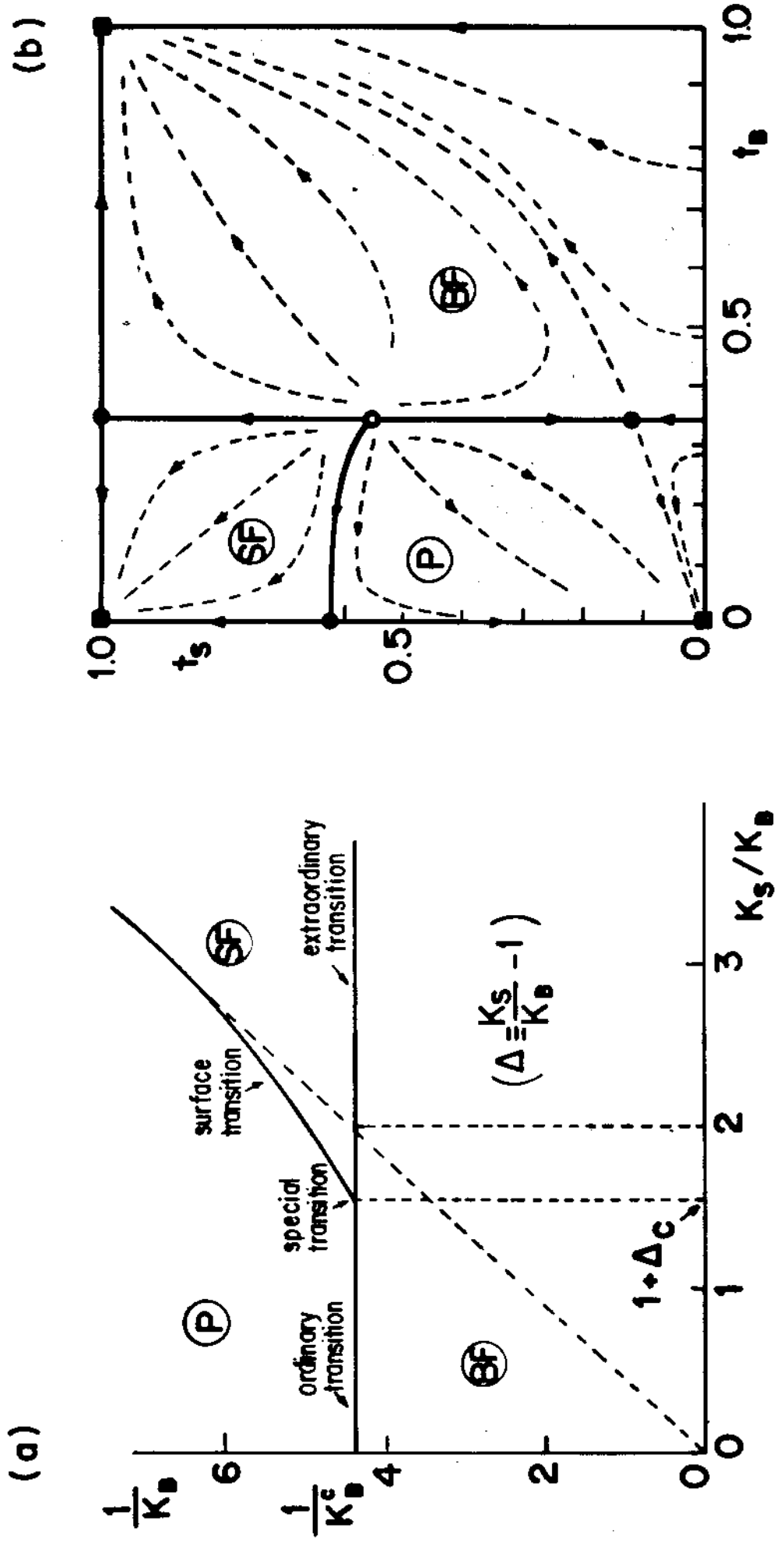
(a)
(b)
SF
P
surface transition
special transition
ordinary transition
extraordinary transition
$(\Delta \equiv \frac{K_S}{K_B} - 1)$
$1+\Delta_c$
$\frac{1}{K_B}$
$\frac{1}{K_B^c}$
K_S/K_B
t_S
t_B

FIG.2

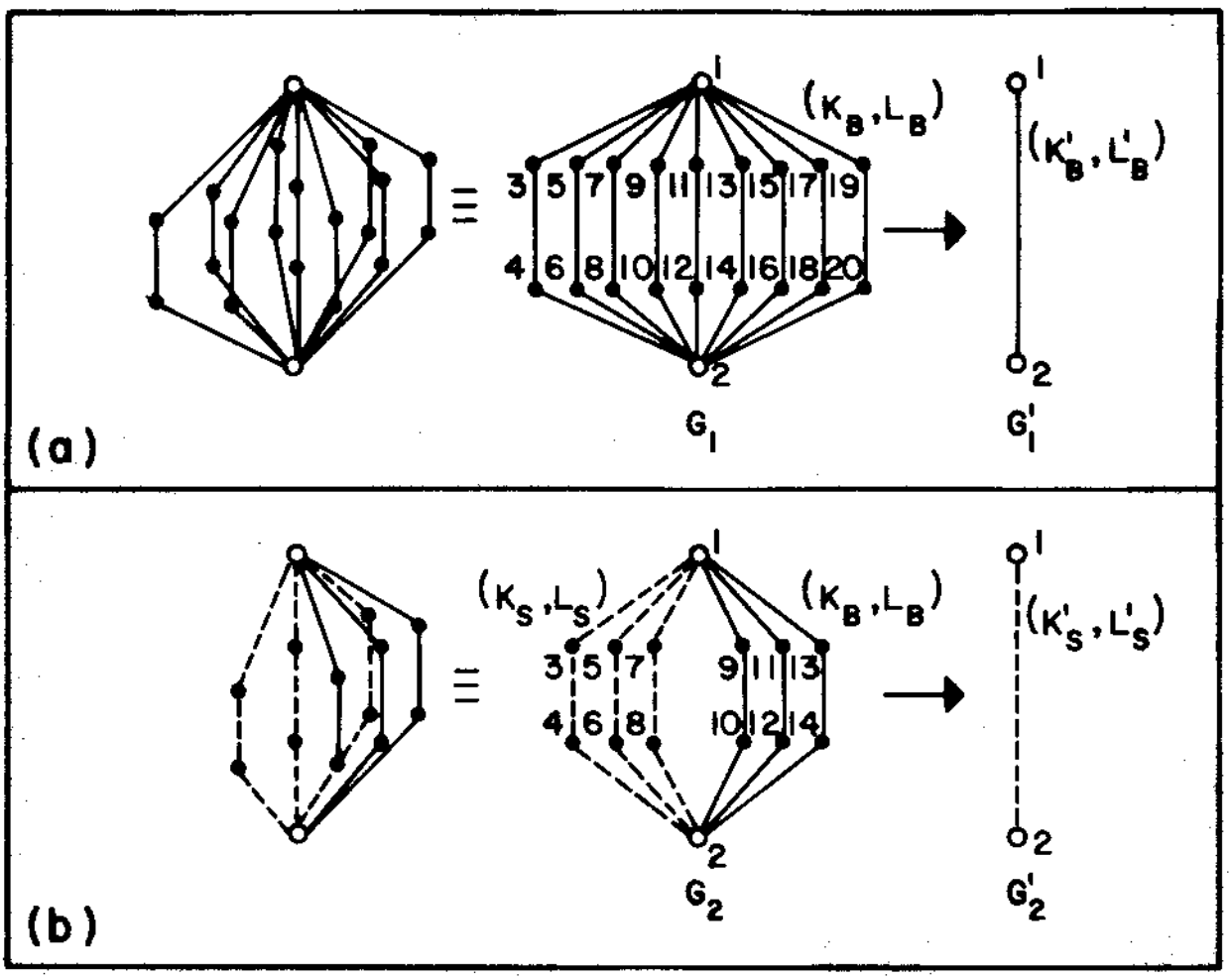
(a)
1
(K_B, L_B)
3 5 7 9 11 13 15 17 19
4 6 8 10 12 14 16 18 20
2
G_1
1
(K'_B, L'_B)
2
G'_1
(b)
1
(K_S, L_S)
(K_B, L_B)
3 5 7 9 11 13
4 6 8 10 12 14
2
G_2
1
(K'_S, L'_S)
2
G'_2

Fig. 3

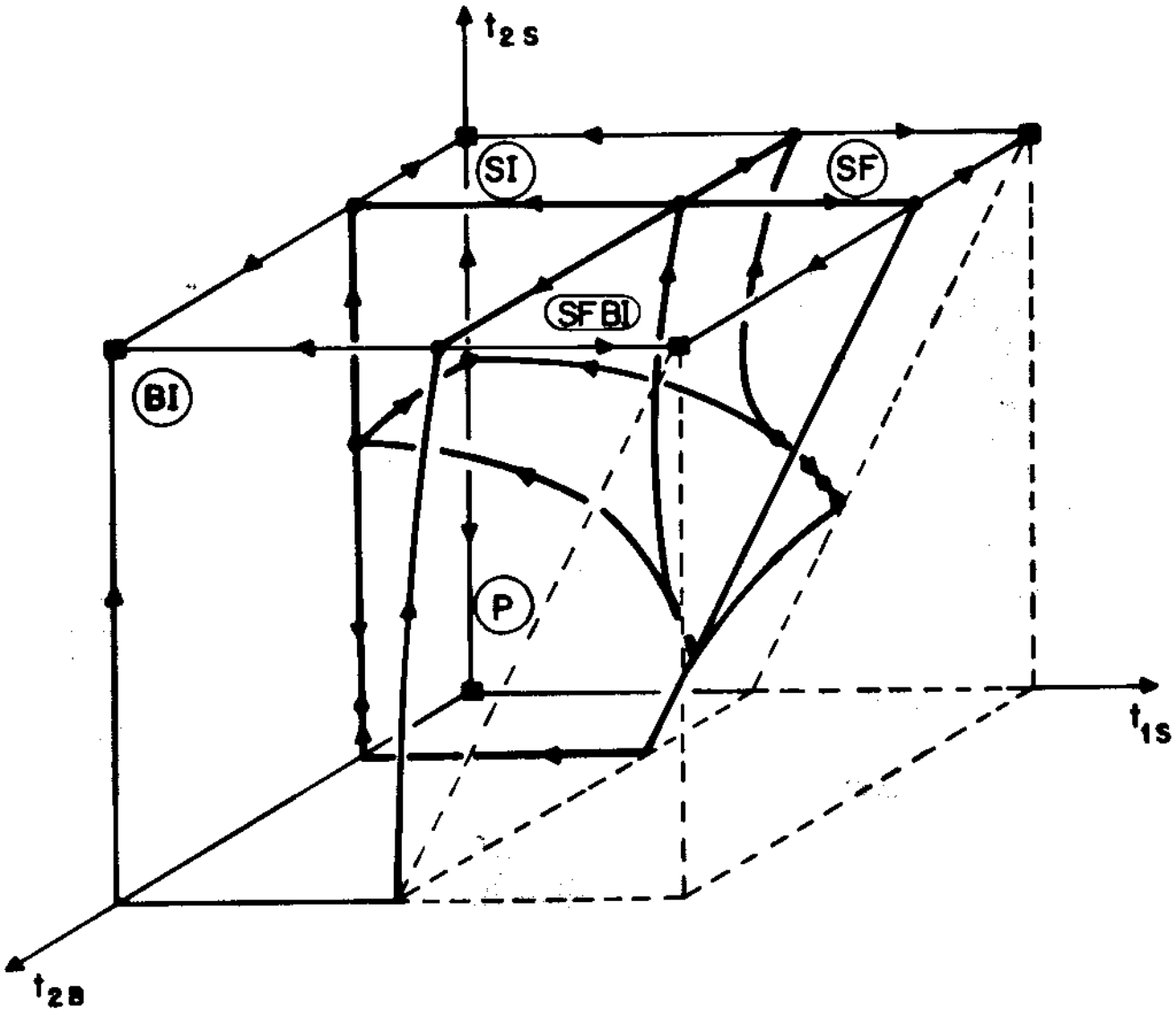

FIG. 4

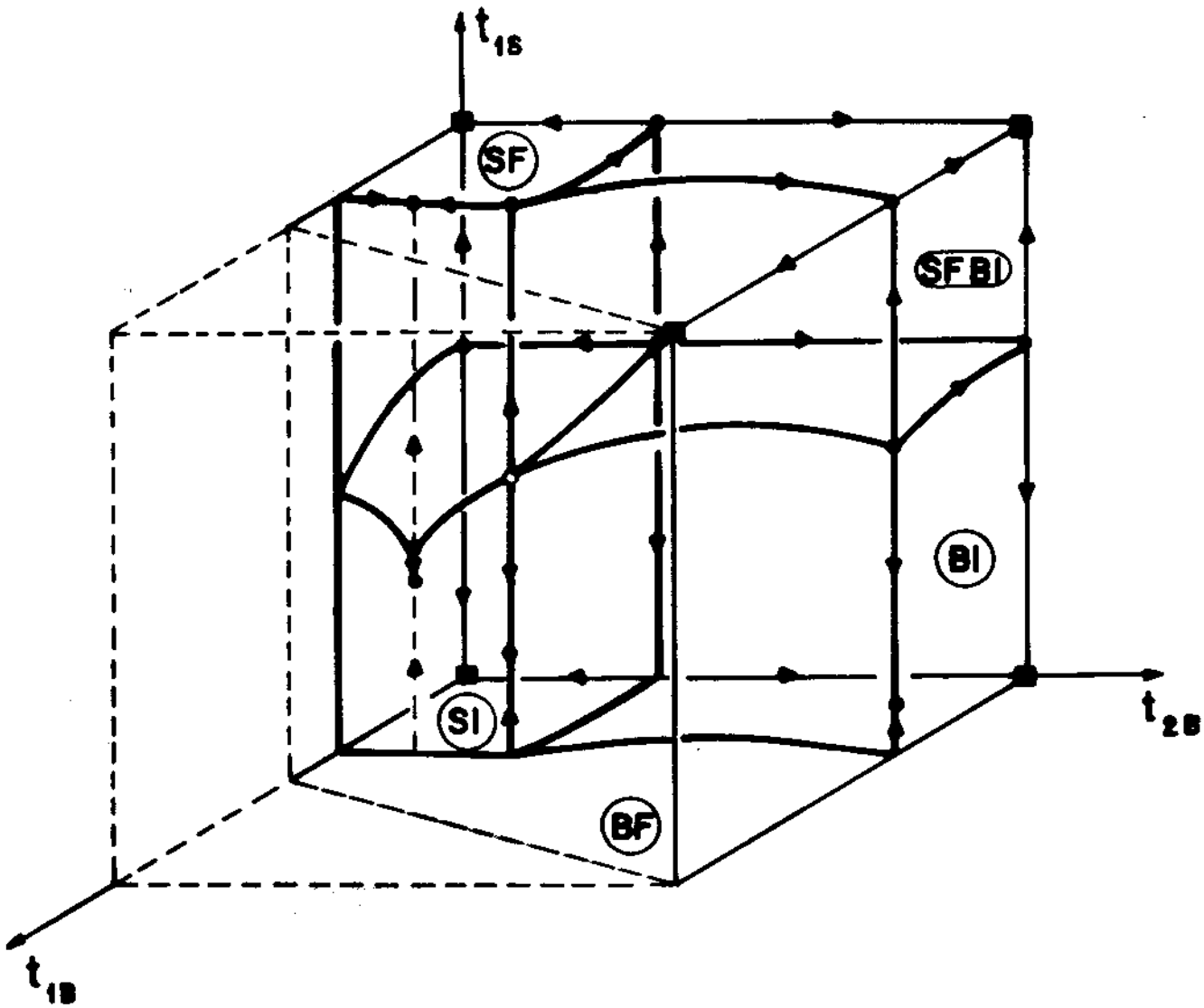

FIG. 5

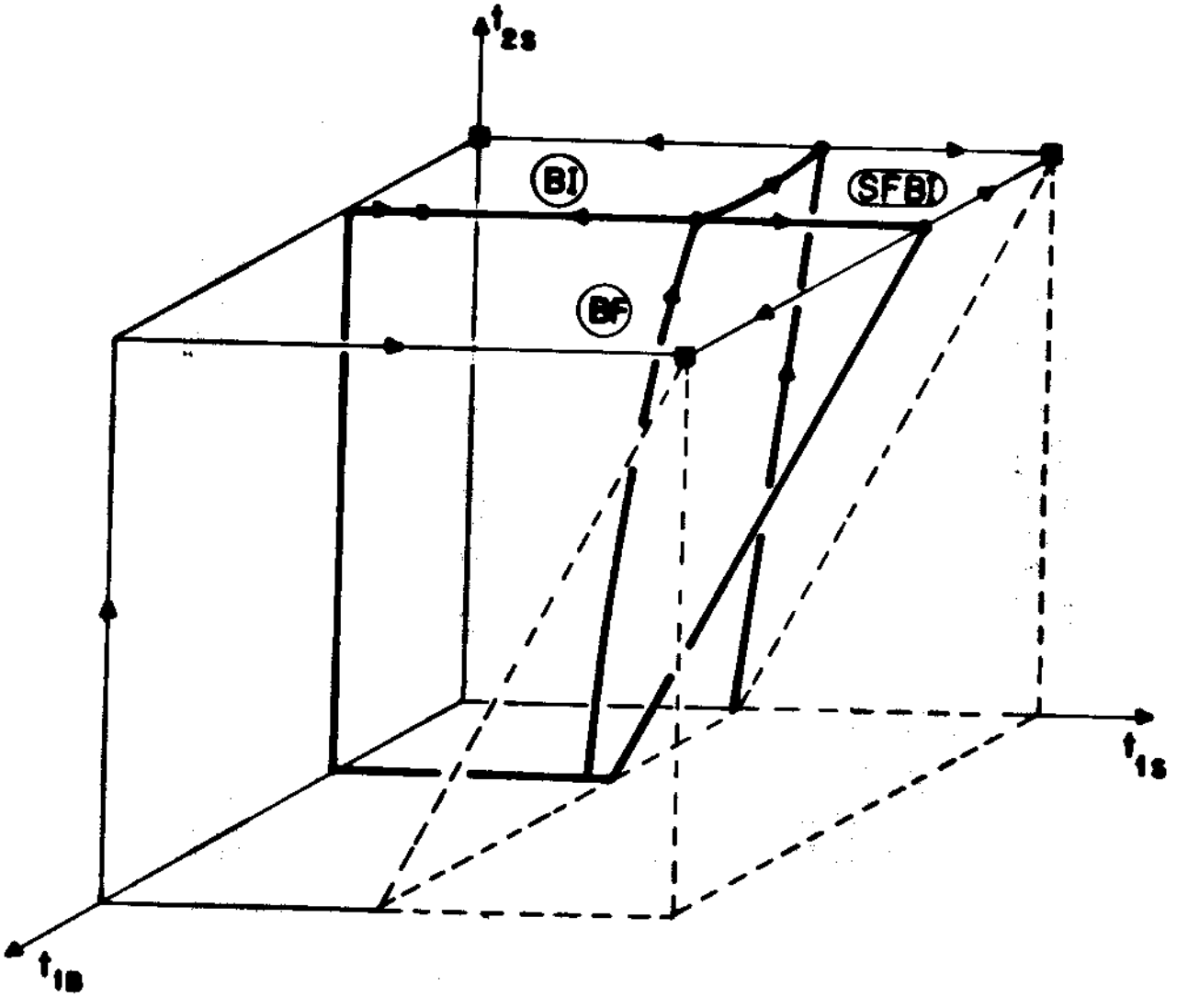

FIG. 6

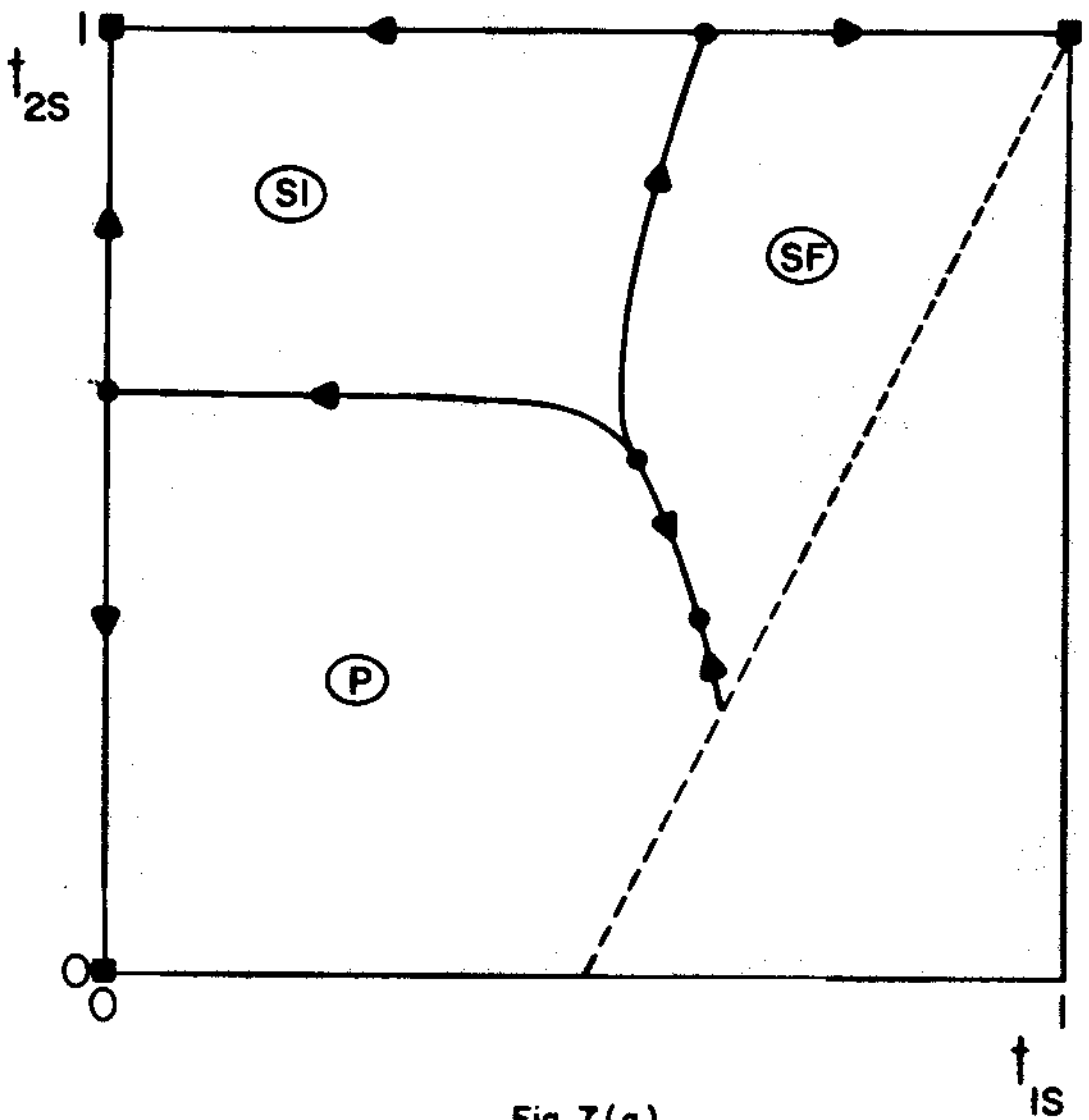

Fig. 7(a)

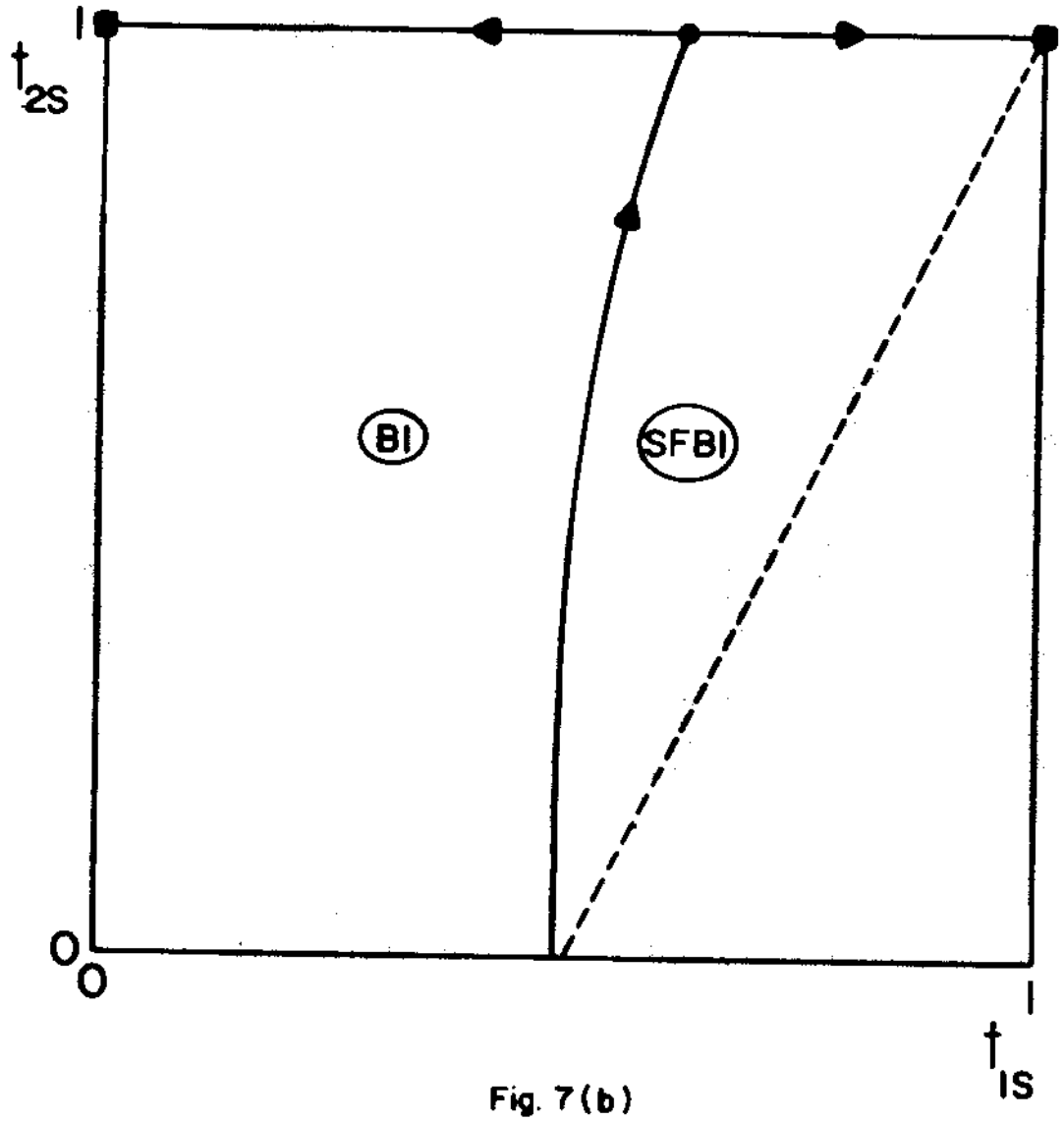

Fig. 7(b)

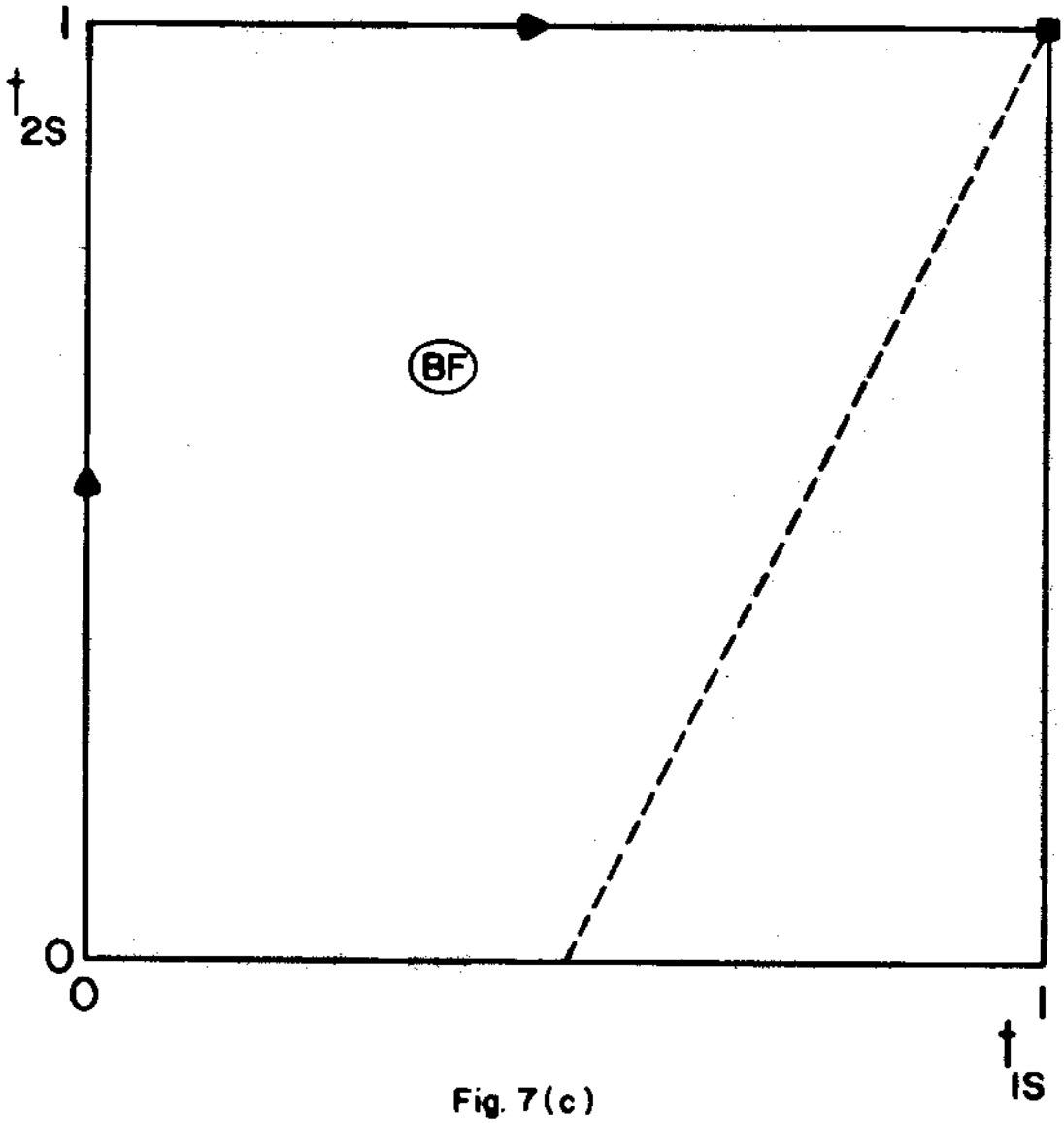

Fig. 7(c)

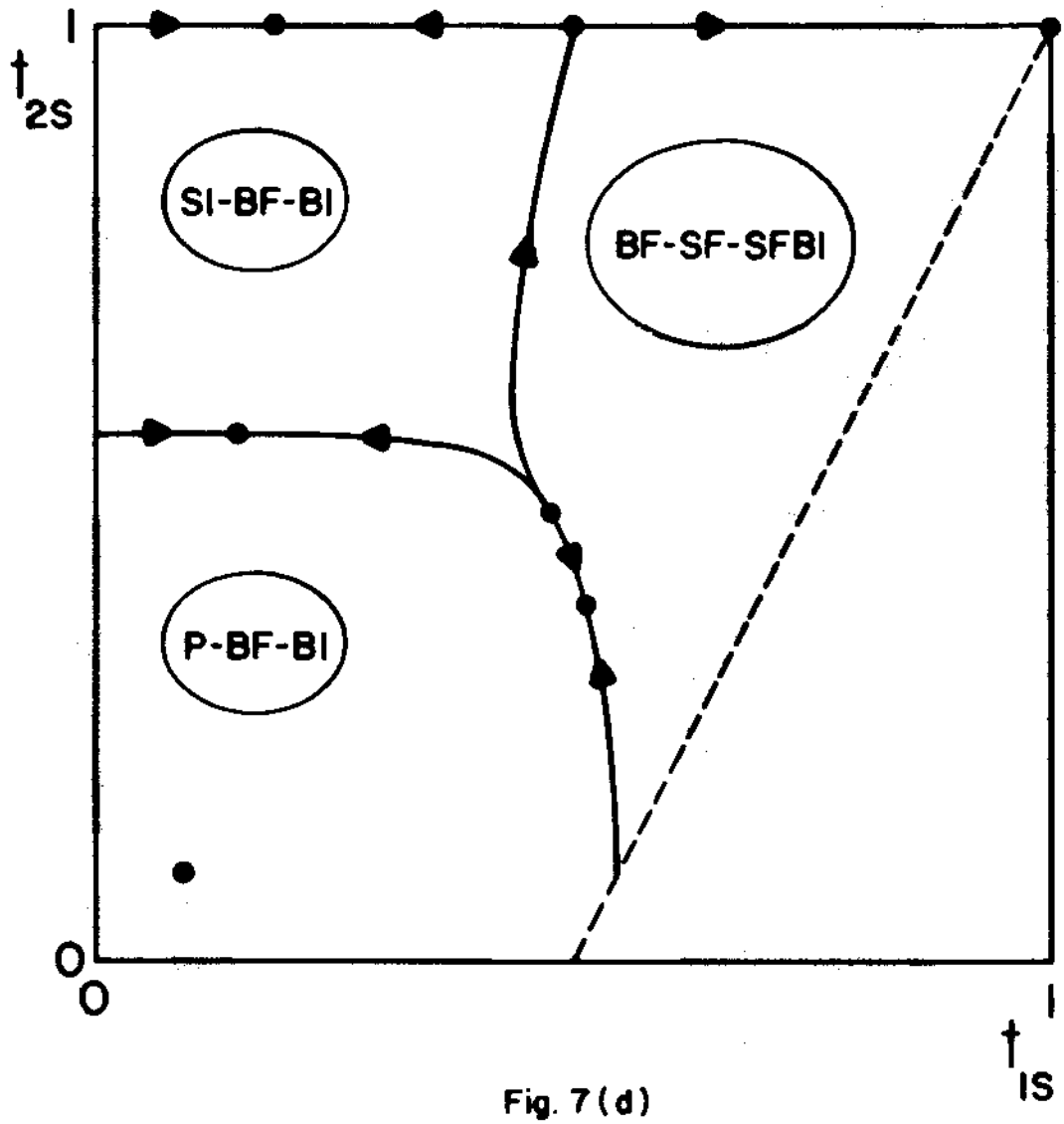

Fig. 7 (d)

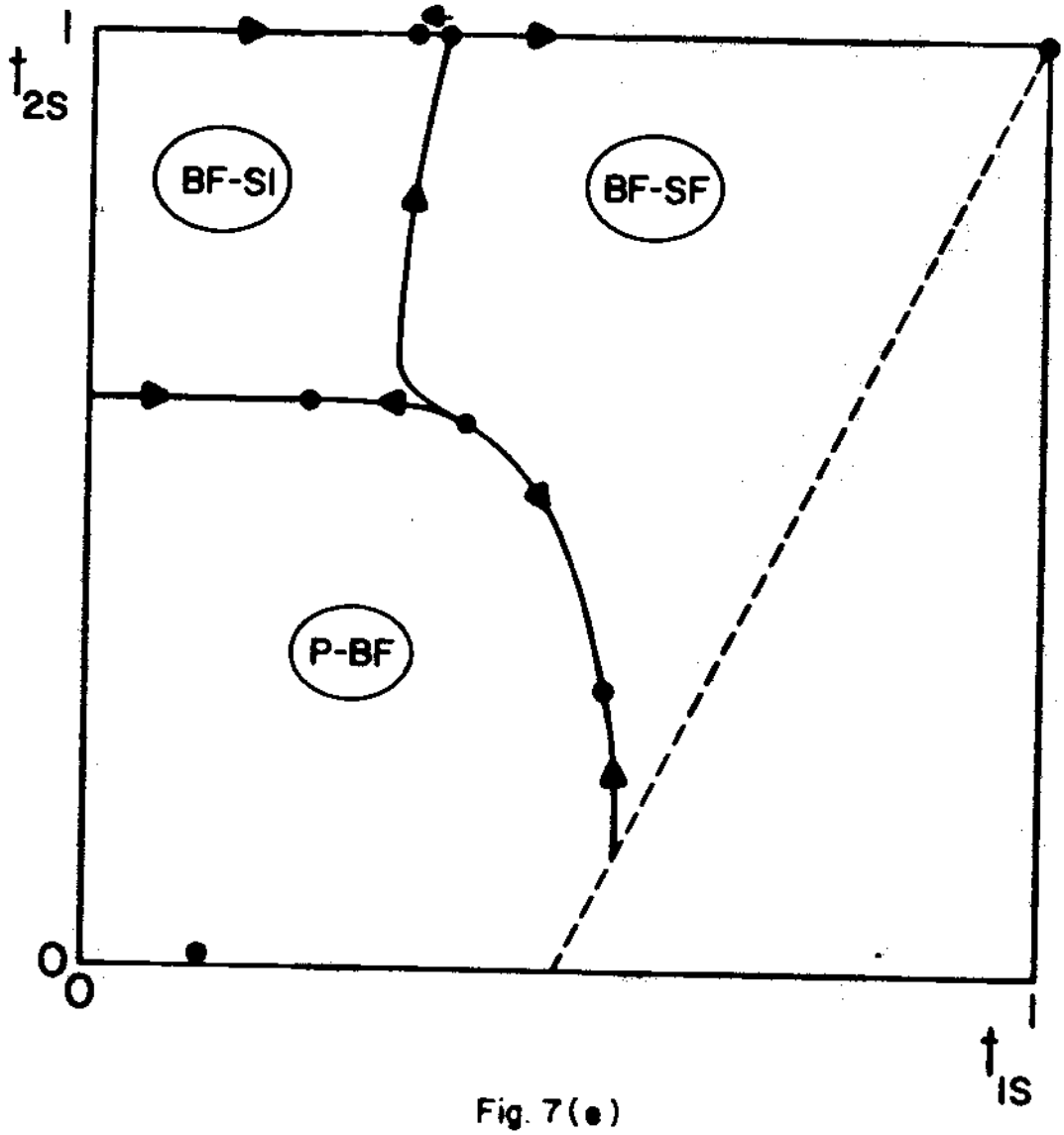

Fig. 7(e)

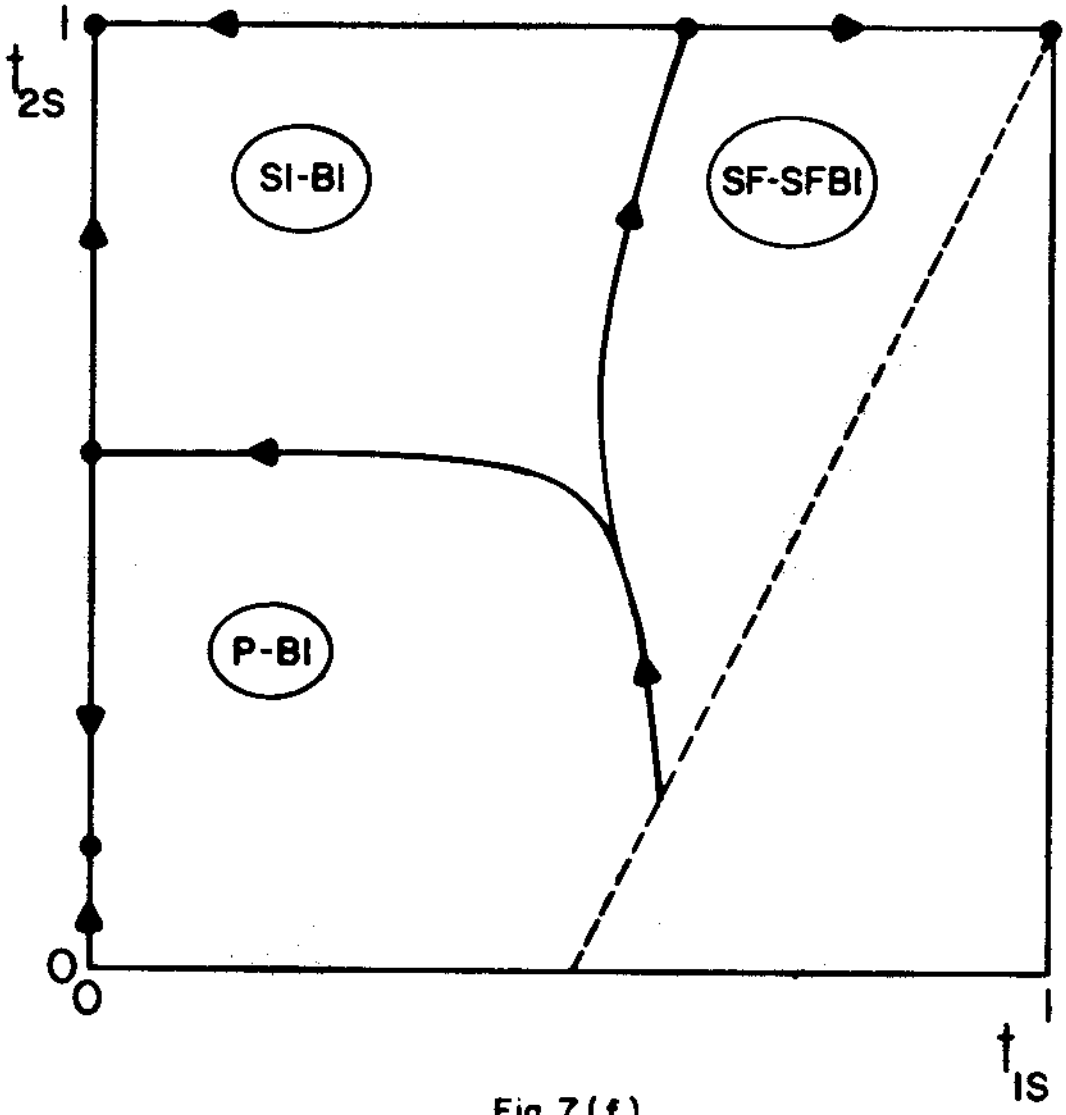

Fig. 7 (f)

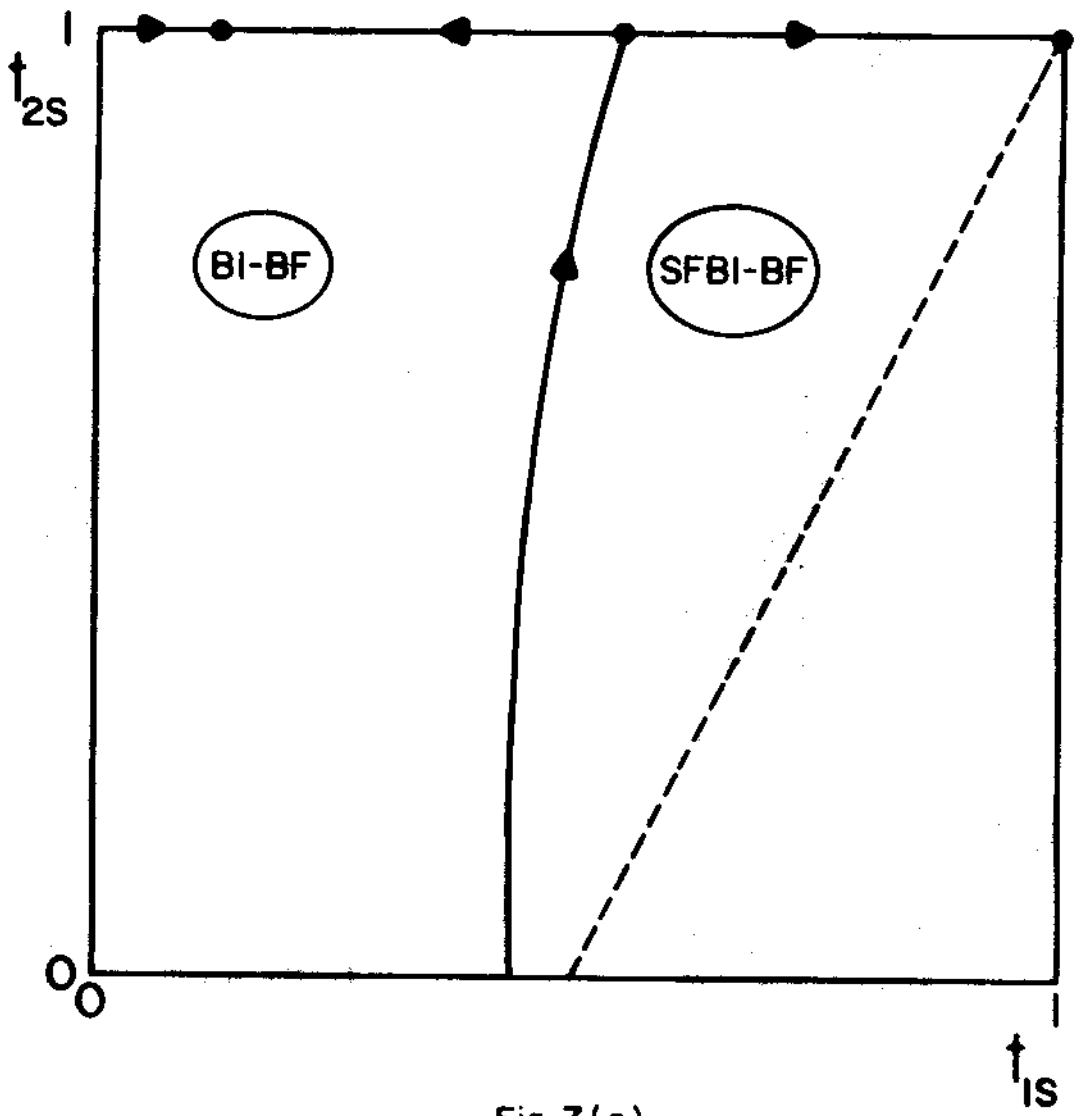

Fig. 7(g)

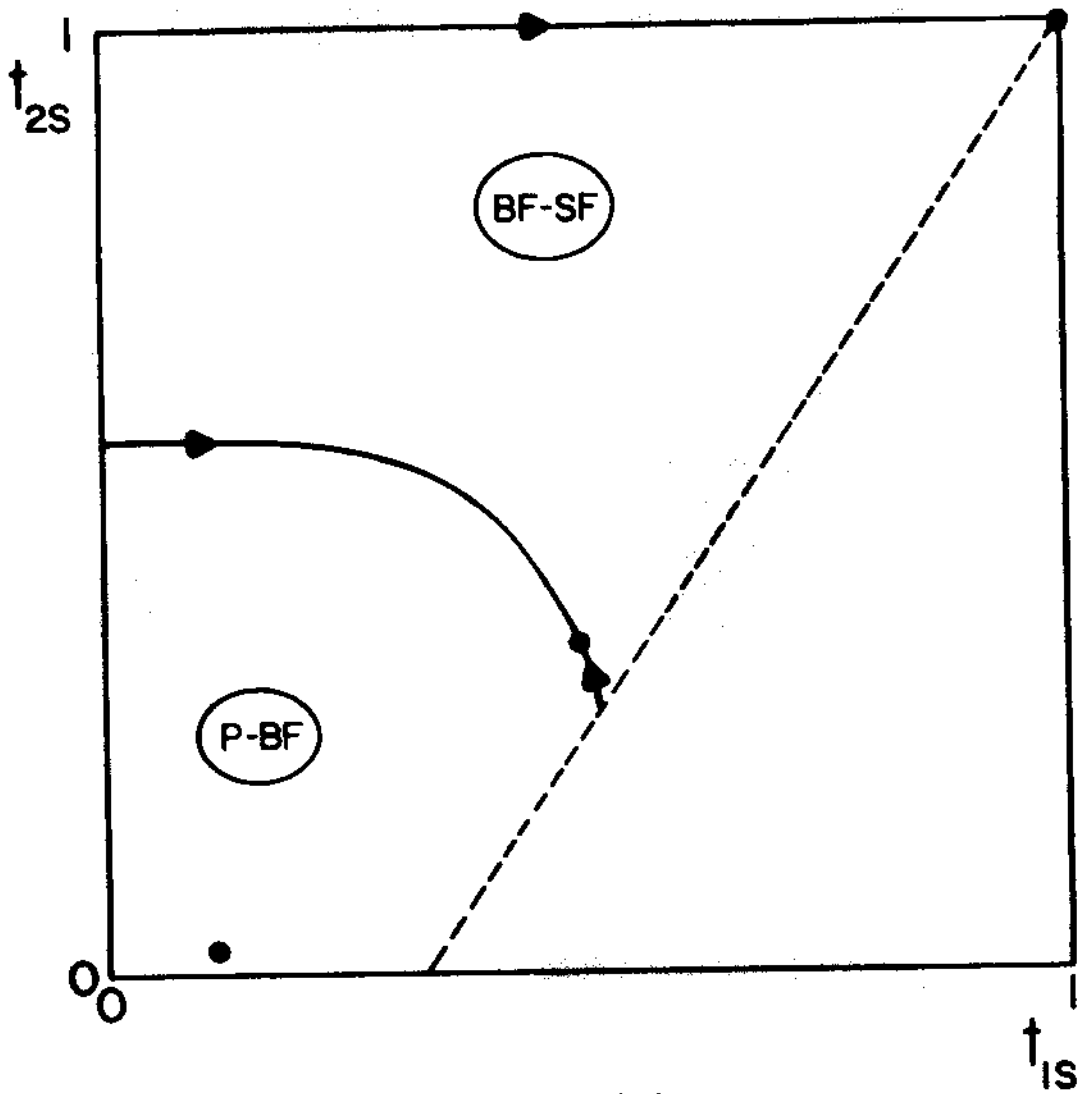

Fig. 7 (h)

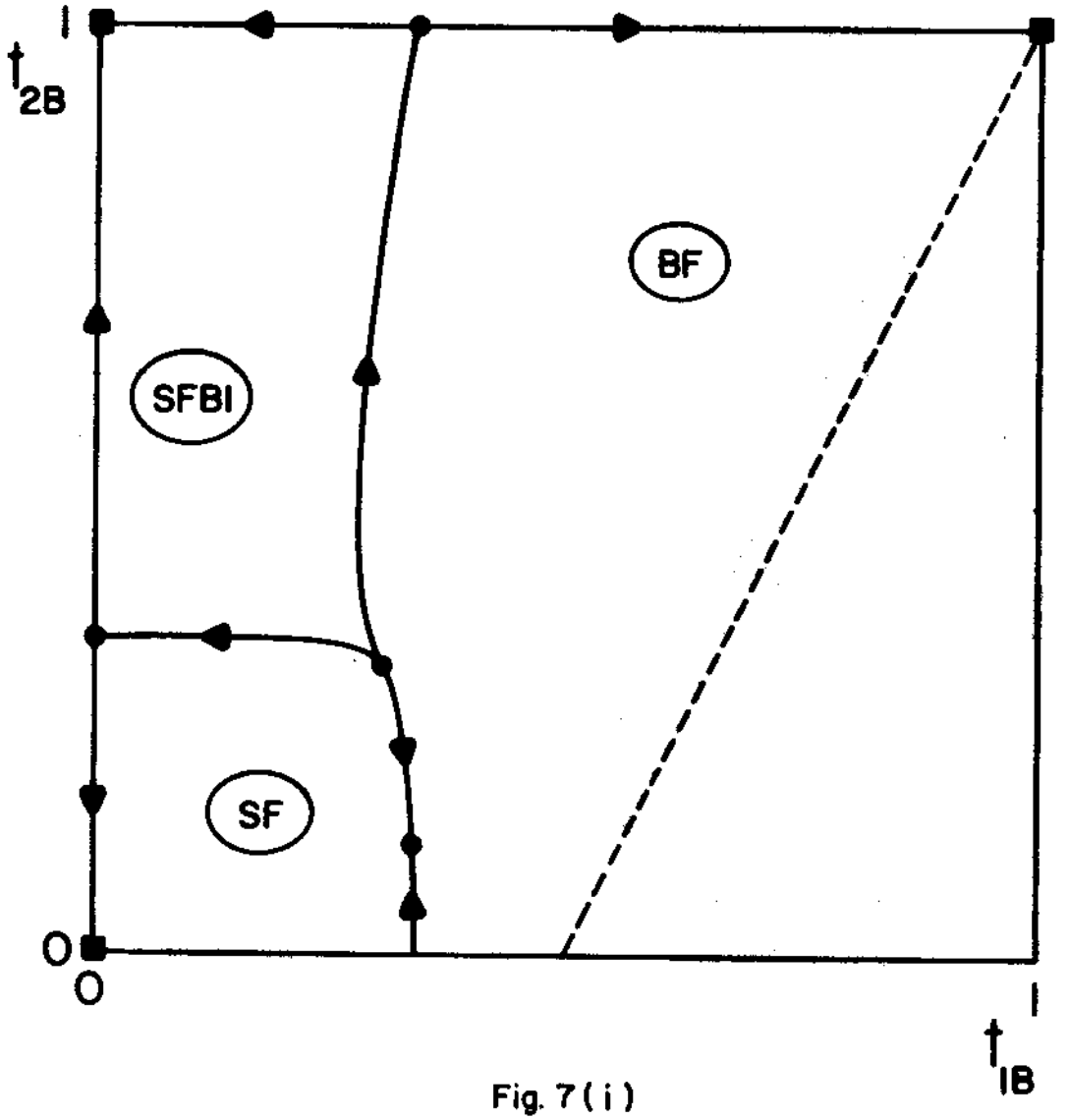

Fig. 7 (i)

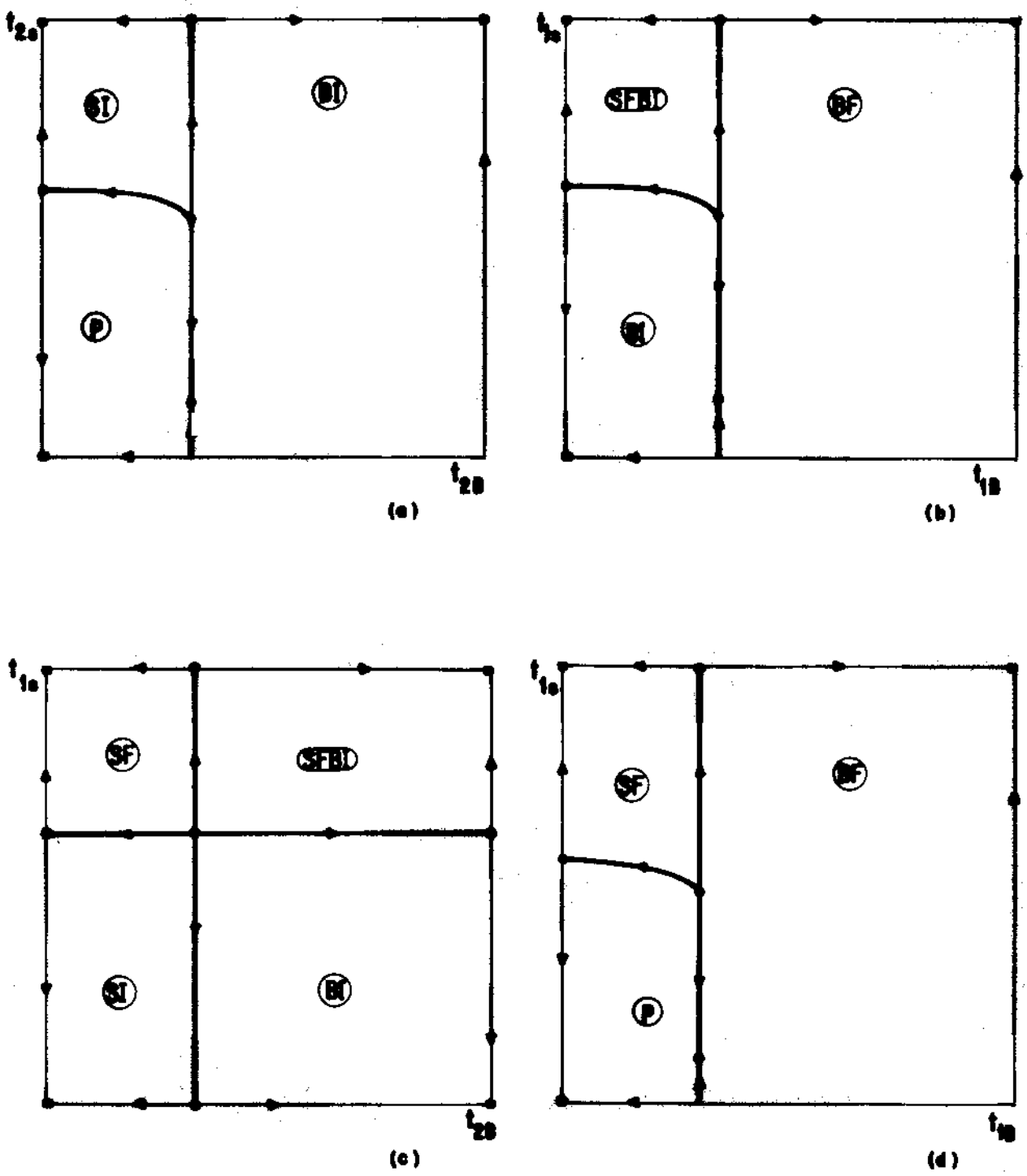
f_{2a}
SI
DI
P
f_{2B}
(a)
f_{1a}
SFBD
BF
SI
f_{1B}
(b)
f_{1a}
SF
SFBD
SI
DI
f_{2B}
(c)
f_{1a}
SF
BF
P
f_{1B}
(d)

FIG. 8

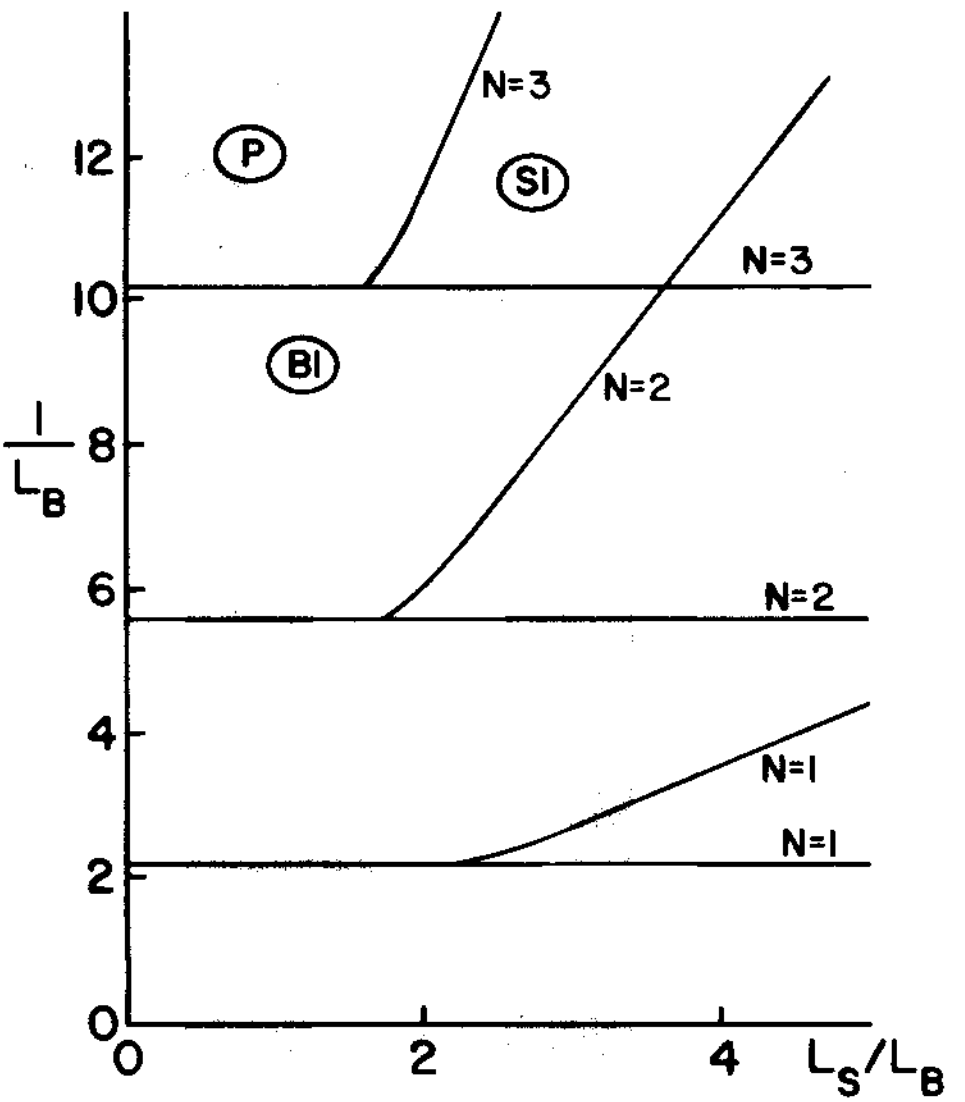

Fig. 9(a)

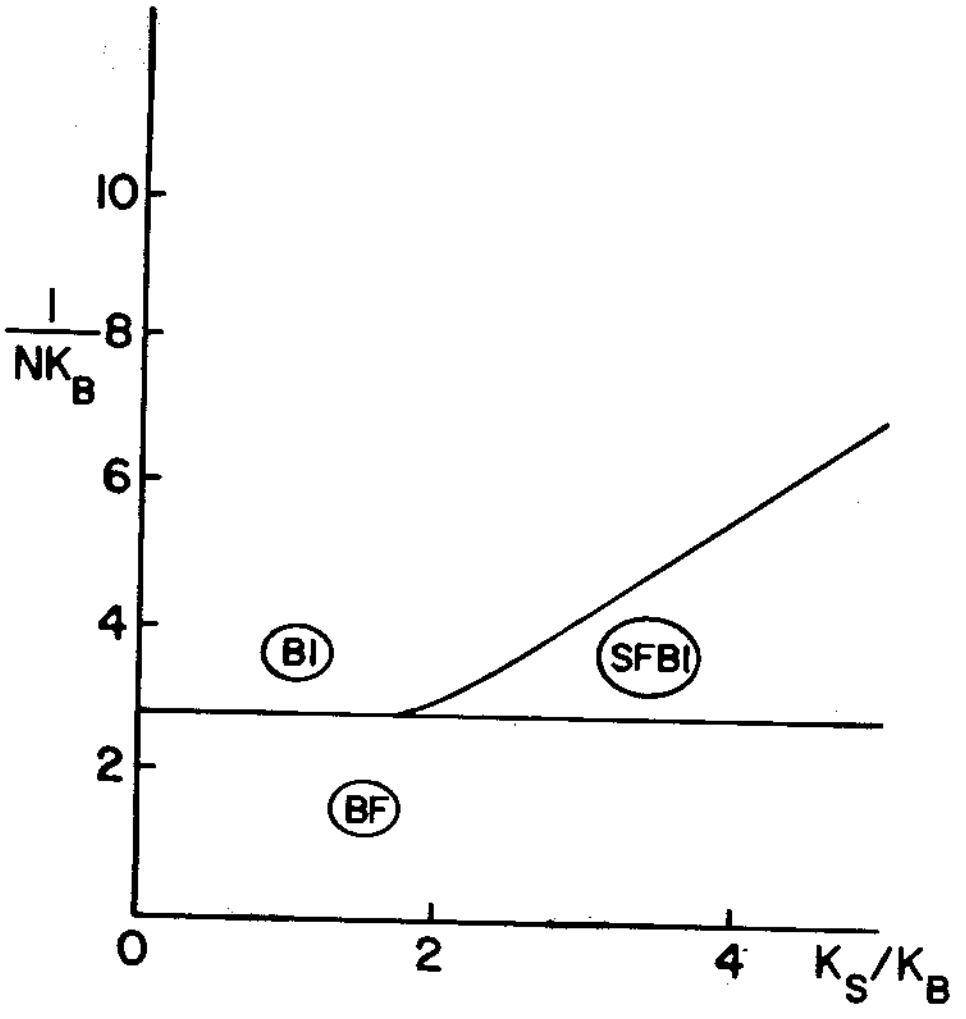

Fig. 9(b)

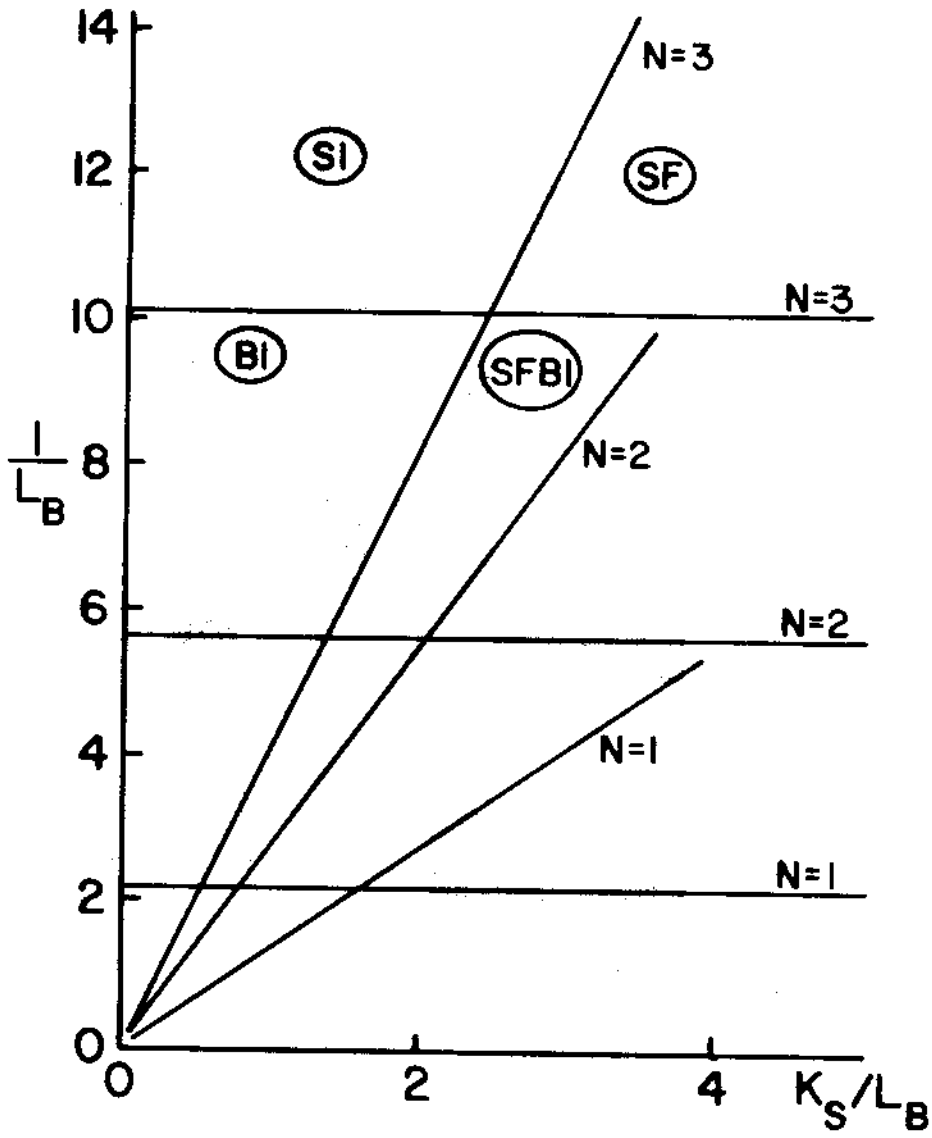

Fig. 9(c)

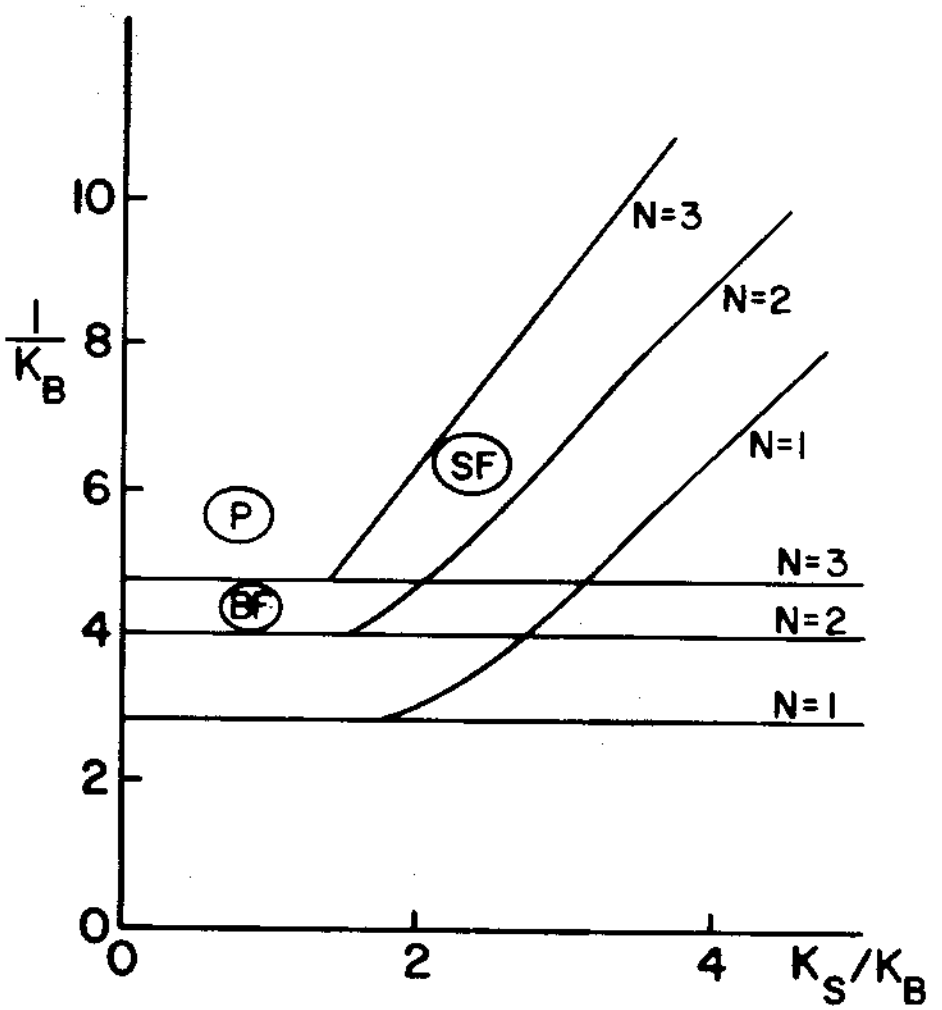

Fig. 9(d)

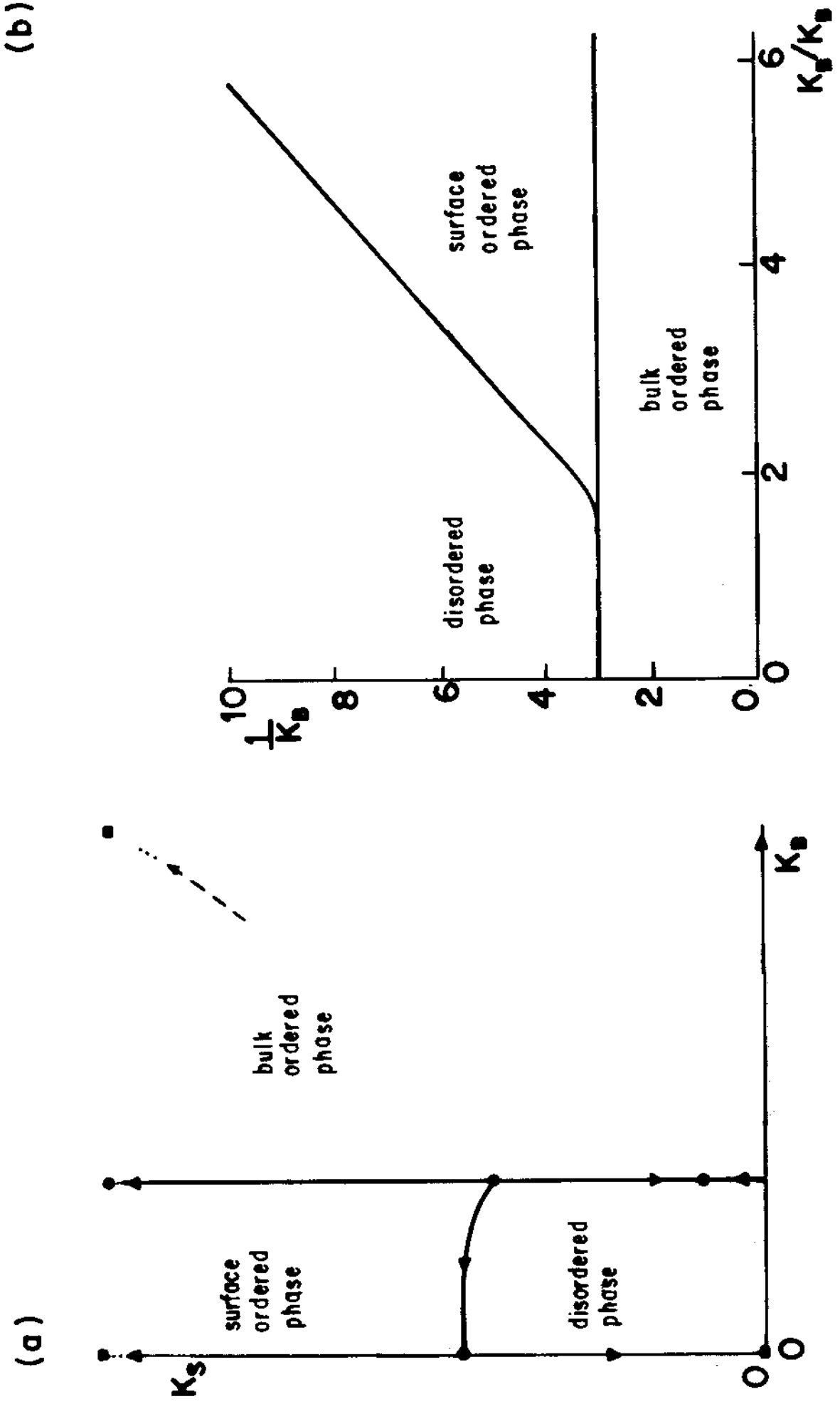
(a)
K_s
surface ordered phase
bulk ordered phase
disordered phase
0
0
K_s
(b)
$\frac{1}{K_s}$
10
8
6
4
2
0
surface ordered phase
disordered phase
bulk ordered phase
0
2
4
6
K_s/K_s

FIG.10

TABLE 1

transition	N = 1	N = 2	N = 3	N → ∞
SI-SF	(0,0,0.62,1) $\nu^{2D} = 1.35$	(0,0,0.62.1) $\nu^{2D} = 1.35$	(0,0,0.62,1) $\nu^{2D} = 1.35$	(0,0,0.62,1) $\nu^{2D} = 1.35$
SF-SFBI	(0,0.37,1,1) $\nu^{3D} = 1.24$	(0,0.34,1,1) $\nu^{3D} = 1.08$	(0,0.32,1,1) $\nu^{3D} = 0.99$	(0,0,1,1) §
SFBI-BI	(0,1,0.62,1) $\nu^{2D} = 1.35$	(0,1,0.62,1) $\nu^{2D} = 1.35$	(0,1,0.62,1) $\nu^{2D} = 1.35$	(0,1,0.62,1) $\nu^{2D} = 1.35$
BI-SI	(0,0.37,0.1) $\nu^{3D} = 1.24$	(0,0.34,0.1) $\nu^{3D} = 1.08$	(0,0.32,0,1) $\nu^{3D} = 0.99$	(0,0,0,1) §
P-BI	(0,0.37,0,0.15) (1.20*) ν^{3D}=1.24(0.88[a])	(0,0.34,0,0.12) (1.04*) ν^{3D}=1.08(0.63[b])	(0,0.32,0,0.11) ν^{3D}=0.99(0.96*)	(0,0,0,0) §
P-SI	(0,0,0,0.68) (1.65*) ν^{2D}=1.64 (4/3[c])	(0,0,0,0.62) (1.37*) ν^{2D}=1.35(1[c])	(0,0,0,0.58) (1.24*) ν^{2D}=1.22(5/6[c])	(0,0,0,0) §
P-SF	(0,0,0.62,0.15) $\nu^{2D} = 1.35$	(0,0,0.62,0.38) $\nu^{2D} = 1.35$	(0,0,0.56,0.44) $\nu^{2D} = 1.11$	(0,0,0,0) §
BF-BI	(0.34,1,0.12,1) $\nu^{3D} = 1.08$	(0.34,1,0.12,1) $\nu^{3D} = 1.08$	(0.34,1,0.12,1) $\nu^{3D} = 1.08$	(0.34,1,0.12,1) $\nu = 1.08$
BF-SI	(0.34,0.05,0.12,1) $\nu^{3D} = 1.08$	(0.34,0.12,0.34,1) $\nu^{3D} = 1.08$	-	-
BF-SFBI	(0,34,1,1,1) $\nu^{3D} = 1.08$	(0.34,1,1,1) $\nu^{3D} = 1.08$	(0.34,1,1,1) $\nu^{3D} = 1.08$	(0.34,1,1,1) $\nu^{3D} = 1.08$
BF-SF	(0.34,0.05,1,1) $\nu^{3D} = 1.08$	(0.34,0.12,1,1) $\nu^{3D} = 1.08$	(0.32,0.17,1,1) $\nu^{3D} = 0.97$	(0,0,1,1) §
P-BF	(0.34,0.05,0.12,0.01) $\nu^{3D} = 1.08$	(0.34,0.12,0.12,0.02) $\nu^{3D} = 1.08$	(0.32,0.17,0.11,0.03) $\nu^{3D} = 0.97$	(0,0,0,0) §

TABLE 2

N	$\mathcal{P}(N)$	$\mathcal{P}(2N)$	$\mathcal{C}$	$\mathcal{I}$
1	(0,0.37)	(0.34,0.34)	(0.34,0.05)	(0.34,1)
2	(0,0.34)	(0.31,0.31)	(0.34,0.12)	(0.34,1)
3	(0,0.32)	(0.29,0.29)	(0.33,0.17)	(0.34,1)
∞	(0,0)	(0,0)	(0,0)	(0.34,1)

TABLE 3

N	multicritical point $(t_{1B}, t_{2B}, t_{1S}, t_{2S})$	$\Delta_c = L_S/L_B - 1$	$1/L_B^c$	ν^{3D}	ϕ^{-1}
1	(0,0.37,0,0.62)	1.11 (1.10*)	2.18	1.24	1.63 (1.68*)
2	(0.0.34,0,0.55)	0.74 (0.76*) (0.6[d],0.5[e])	5.65	1.08	1.53 (1.54*) (1.47[f])
3	(0,0.32,0,0.51)	0.59 (0.63*)	10.2	0.99	1.50 (1.49*)
∞	(0,0,0,0)			§	-

TABLE 4

N	multicritical point $(t_{1B}, t_{2B}, t_{1S}, t_{2S})$	$\Delta_c = K_S/K_B - 1$	$1/K_B^c$	ν^{3D}	$\phi^{\pm 1}$
any	(0.34,1,0.55,1)	0.74 (0.76*)	2.82	1.08	1.53 (1.54*)

TABLE 5

N	multicritical point $(t_{1B}, t_{2B}, t_{1S}, t_{2S})$	$\Delta_c = K_S/K_B - 1$	$1/L_B^c$	ν^{3D}	ϕ^{-1}
1	(0,0.37,0.62,1)	0.58	2.18	1.24	1.09
2	(0,0.34,0.62,1)	1.04	5.65	1.08	1.25
3	(0,0.32,0.62,1)	1.45	10.2	0.99	1.36
∞	(0,0,0.62,1)		-	§	

TABLE 6

N	multicritical point $(t_{1B},t_{2B},t_{1S},t_{2S})$	$\Delta_c=K_S/K_B-1$	$1/K_B^c$	ν^{3D}	ϕ^{-1}	semi-stable fixed point P-SI-SF	ν^{2D}	semi-stable fixed point SF-SFBI-BF and P-BI-BF	ν^{3D}
1	(0.34,0.34,0.55,0.55)	0.74	2.82	1.08 (1.04*) (0.63[b])	1.53	(0,0,0.62,0.62)	1.35 (1.37*) (1[c])	(0.34,0.34,1,1) and (0.34,0.34,0.12,0.12)	1.08 (1.04*) (0.63[b])
2	(0.31,0.31,0.48,0.48)	0.51	1.96	0.94	1.48	(0,0,0.55,0.55)	1.15	(0.31,0.31,1,1) and (0.31,0.31,0.10,0.10)	0.94
3	(0.029,0.29,0.44,0.44)	0.42	1.62	0.87	1.45	(0,0,0.51,0.51)	1.05	(0,29,0.29,1,1) and (0.29,0.29,0.08,0.08)	0.87
∞	(0,0,0,0)			§		(0,0,0,0)	§	(0,0,1,1) and (0,0,0,0)	§

REFERENCES

1) Bruce, A.D. and Aharony, A., Phys. Rev. B 11 (1975) 478.

2) Aharony, A. and Bruce, A.D., Proc. 20th A. Conf. on Magnetism and Magnetic Materials, San Francisco 1974: AIP Conf. Press. No 24 (1975) p.296.

3) Kim, D., Levy, P.M. and Uffer, L.F., Phys. Rev. B 12 (1975) 989.

4) Schick, M., Surf. Sci. 125 (1983) 94.

5) Harris, A.B. and Berlinsky, A.J., Can. J. Phys. 57 (1979) 1852.

6) Chung, T.T. and Dash, J.G., Surf. Sci. 66 (1977) 559; Eckert, J. Ellenson, W.D., Hastings, J.B. and Passel, L.L. Phys. Rev. Lett. 43 (1979) 1329; Diehl, R.D., Toney, M.F. and Fain. Jr., S.C. Surf. Sci. 125 (1983) 116.

7) Hilhorst, H.J., Phys. Rev. B 16 (1977) 1253.

8) Domany, E. and Riedel, E.K., Phys. Rev. B 19 (1979) 5817.

9) Nienhuis, B., Riedel, E.K., and Schick, M., Phys. Rev. B 27, (1983) 5625.

10) Badke, R., Reinick, P. and Rittenberg, V., J. Phys. A: Math. Gen. 18 (1985) 653.

11) von Gehlen, G. and Rittemberg, V., J. Phys. A: Math. Gen. 19 (1986) 2439.

12) Badke, R., Phys. Lett. A 119 (1987) 365.

13) Tsallis, C., Mariz, A.M., Stella, A. and da Silva, L.R., to appear in J. Phys. A: Math. Gen. 22 (1989).

14) Mariz, A.M., Tsallis, C. and Fulco, P., Phys. Rev. B 32 (1985) 6055.

15) Kim, D. and Levy, P.M.,Phys. Rev. B 12 (1975) 5105.

16) Aharony, A., J.,Phys. A: Math. Gen. 10 (1977) 389.

17) Tsallis, C. and Sarmento, E.F., J. Phys. C 18 (1985) 2777.

18) Essam, J.W. and Tsallis, C.,J. Phys. A: Math. Gen. 19 (1986) 409.

19) Costa, U.M.S., Tsallis, C. and Sarmento, E.F.,J. Phys. C 18 (1985) 5749.

20) Heerman, D.W. and Stauffer, D., Z. Phys. B 44 (1981) 339.

21) Le Guillou, J.C. and Zinn-Justin, J.,Phys. Rev. B 21 (1980) 3976.

22) den Nijs, M.P.M.,Physica 95 A (1979) 449.

23) Binder, K. and Hohenberg, P.C., Phys. Rev. B 9 (1974) 2194.

24) Binder, K. and Landau, D.P.,Phys. Rev. Lett. 52 (1984) 318.

25) Diehl, H.W. and Dietrich, S.,Phys. Lett. 80 A (1980) 408.